Brown University
DIVISION OF ENGINEERING
PROVIDENCE, R.I. 02912

Microscopic Observations of Adiabatic Shear Bands in Three Different Steels

K. Cho, Y.C. Chi and J. Duffy
Division of Engineering, Brown University
Providence, R.I. 02912

UNCLASSIFIED
SECURITY CLASSIFICATION OF THIS PAGE

ADA202522

REPORT DOCUMENTATION PAGE

1a. REPORT SECURITY CLASSIFICATION: Unclassified	1b. RESTRICTIVE MARKINGS
2a. SECURITY CLASSIFICATION AUTHORITY	3. DISTRIBUTION / AVAILABILITY OF REPORT: Approved for public release; distribution unlimited.
2b. DECLASSIFICATION / DOWNGRADING SCHEDULE	
4. PERFORMING ORGANIZATION REPORT NUMBER(S): 3	5. MONITORING ORGANIZATION REPORT NUMBER(S): ARO 25544.4-EG
6a. NAME OF PERFORMING ORGANIZATION: BROWN UNIVERSITY; 6b. OFFICE SYMBOL (If applicable)	7a. NAME OF MONITORING ORGANIZATION: U. S. Army Research Office
6c. ADDRESS (City, State, and ZIP Code): 182 Hope Street B&H 6S, Providence, RI 02912	7b. ADDRESS (City, State, and ZIP Code): P. O. Box 12211, Research Triangle Park, NC 27709-2211
8a. NAME OF FUNDING / SPONSORING ORGANIZATION: U. S. Army Research Office; 8b. OFFICE SYMBOL (If applicable)	9. PROCUREMENT INSTRUMENT IDENTIFICATION NUMBER
8c. ADDRESS (City, State, and ZIP Code): P. O. Box 12211, Research Triangle Park, NC 27709-2211	10. SOURCE OF FUNDING NUMBERS: PROGRAM ELEMENT NO. / PROJECT NO. / TASK NO. / WORK UNIT ACCESSION NO.

11. TITLE (Include Security Classification)
"Microscopic Observations of Adiabatic Shear Bands In Three Different Steels"

12. PERSONAL AUTHOR(S)
K. Cho, Y.C. Chi and J. Duffy

13a. TYPE OF REPORT	13b. TIME COVERED	14. DATE OF REPORT (Year, Month, Day)	15. PAGE COUNT
Technical	FROM _____ TO _____	September, 1988	48

16. SUPPLEMENTARY NOTATION
The view, opinions and/or findings contained in this report are those of the author(s) and should not be construed as an official Department of the Army position, policy, or decision, unless so designated by other documentation.

17. COSATI CODES		
FIELD	GROUP	SUB-GROUP

18. SUBJECT TERMS (Continue on reverse if necessary and identify by block number)
Adiabatic Shear Bands, Steels, ~~1018 CRS, HY-100 Steel, 4340 VAR~~ steel, Fractography, Voids, and Microcracks. (Mgm)

19. ABSTRACT (Continue on reverse if necessary and identify by block number)

Microscopic observations are made of the shear band material in three different steels: (1) an AISI 1018 cold rolled steel, (2) a high strength low alloy structural steel, and (3) an AISI 4340 VAR steel tempered to either of two hardnesses, RHC 44 or 55. Dynamic deformation in shear was imposed to produce shear bands in all the steels tested. It was found that whenever the shear band led to fracture of the specimen, the fracture occurred by a process of void nucleation and coalescence; no cleavage was observed on any fracture surface, including the most brittle of the steels tested (RHC = 55). This is presumably due to the softening of the shear band material that results from the local temperature rise occurring during dynamic deformation. Differences in shear band behavior between the various microstructures are also described.

20. DISTRIBUTION / AVAILABILITY OF ABSTRACT	21. ABSTRACT SECURITY CLASSIFICATION
☐ UNCLASSIFIED/UNLIMITED ☐ SAME AS RPT ☐ DTIC USERS	Unclassified
22a. NAME OF RESPONSIBLE INDIVIDUAL: Professor J. Duffy	22b. TELEPHONE (Include Area Code) / 22c. OFFICE SYMBOL

DD FORM 1473, 84 MAR — 83 APR edition may be used until exhausted. All other editions are obsolete

SECURITY CLASSIFICATION OF THIS PAGE
UNCLASSIFIED

Microscopic Observations of Adiabatic Shear Bands in Three Different Steels

K. Cho, Y.C. Chi and J. Duffy
Division of Engineering, Brown University
Providence, R.I. 02912

Army Research Office
Report No. DAAL03-88-K-0015/3

Material Research Laboratory
Brown University
September, 1988

September, 1988

Microscopic Observations of Adiabatic Shear Bands in Three Different Steels

by

K. Cho[1], Y.C. Chi[2], and J. Duffy[3]
Division of Engineering
Brown University
Providence, RI 02912

Abstract

Microscopic observations are made of the shear band material in three different steels: (1) an AISI 1018 cold rolled steel, (2) a high strength low alloy structural steel, and (3) an AISI 4340 VAR steel tempered to either of two hardnesses, RHC 44 or 55. Dynamic deformation in shear was imposed to produce shear bands in all the steels tested. It was found that whenever the shear band led to fracture of the specimen, the fracture occurred by a process of void nucleation and coalescence; no cleavage was observed on any fracture surface, including the most brittle of the steels tested (RHC = 55). This is presumably due to the softening of the shear band material that results from the local temperature rise occurring during dynamic deformation. Differences in shear band behavior between the various microstructures are also described.

[1] Research Associate
[2] Research Assistant
[3] Professor of Engineering

A. Introduction

The formation of narrow zones of highly localized deformation, known as shear bands, is an important phenomenon frequently occurring when materials are deformed at high strain rates. Whether or not it is accompanied by fracture, this localization generally implies failure of the structural component through an essentially complete loss in the load-carrying capacity of the highly deformed material within the shear band [1-4]. It has been reported that localization occurs more readily in materials with a low strain hardening rate, a low strain rate sensitivity, a low thermal conductivity, and a high thermal softening rate. Examples include alloys of titanium, aluminum, copper, as well as steels [5-22]. Shear bands have been observed in many practical applications involving dynamic deformation including machining, ballistic impact and high velocity shaping and forming. Attesting to the significance of shear banding is the large number of recent studies, including experimental observations, analytical modeling and metallurgical investigations. These are reviewed by Argon [23], Rogers [24,25], Bedford, Wingrove and Thompson [26], Clifton [27], Olson, Mescall and Azrin [28], Hutchinson [29], and Timothy [30]. Backman and Finnegan [31] have classified shear bands into either of two types, deformed and transformed, depending upon whether or not a phase transformation has occurred. According to this classification, transformed bands may be as narrow as 5 or 10 microns and will appear white when etched with a nital solution; in contrast deformed bands, while showing an enhanced local deformation, generally remain fairly broad and do not etch white.

Recent modeling of shear band initiation has concentrated on the role of defects, particularly geometric or dimensional variations, temperature differences, and the role of inclusions. Thus, Molinari and Clifton [32] predicted critical conditions for shear band formation by considering the size of geometrical defects, while Wright and Walter [33] concentrated on a temperature inhomogeneity to trigger the shear band.

The present paper describes types of fracture that occur during shear band formation as they relate to metallurgical factors. Recently, experiments have been performed to study details of the formation process of shear bands [1,2]. These include local temperature measurements, effected by means of infra-red detectors, which have measured a temperature rise in excess of 600°C within the region of the shear band. They also include microsecond exposure photographs of the shear band formation process. The latter tests are aimed at measuring localized strain both as a function of time and as a function of position on the metal surface. All the experiments in question in these investigations make use of a torsional Kolsky bar (torsional split-Hopkinson bar) to deform thin-walled tubular specimens of the various steels. The method is described in References [1] to [4]. The dynamic strain rate imposed in these tests is about 10^3/s in shear. Throughout these investigations, the role of microstructure (e.g. the grain boundaries, phase boundaries, precipitates, inclusions, etc.) may also be considered as one of the important factors in the formation of the shear band [17,34]. These microstructural inhomogeneities can provide initiation sites for the voids and microcracks which lead to the process of shear band formation and eventually to failure of the material.

For the present paper, microscopic examinations were made of shear bands in three different steels: an AISI 1018 cold rolled steel (CRS), HY-100 structural steel and AISI 4340 VAR steel subjected to two different heat treatments. Under present experimental conditions and, in particular, at strain rate of about 10^3/s, the shear bands in 1018 CRS are of the deformed type. With continued straining voids initiate at the ferrite-pearlite boundaries within these shear bands, apparently as a result of the cracking of thin pearlites. Propagation and linkage of the microcracks follows along the phase boundaries. Shear bands in HY-100 steel initially are of the deformed type but, at larger strains, give evidence of a narrower band that etches white. The voids within the shear bands in this steel nucleate at manganese sulfide,

MnS, inclusions. Their coalescence eventually can result in fracture along the shear band, although in many tests no fracture was seen even though the dynamic stress level dropped sharply [1-4]. Two microstructures of AISI 4340 VAR were tested and each formed shear bands of the transformed type. The fracture surface within the transformed shear bands showed ductile dimples presumably forming at carbide particles. They indicate that the fracture process is fibrous, probably because of the temperature rise within the shear band. No evidence of void formation was observed on the polished surface of the shear band, but observations were limited to SEM and optical microscopy.

B. Description of Experiments

1. General

The chemical composition of the steels is given in Table 1. AISI 1018 CRS and HY-100 were tested in the as-received condition. Two tempers of the AISI 4340 VAR steel were tested; their complete heat-treatment is described in Reference [35]. A temper of 425°C gives a hardness of 44 on the Rockwell C scale, while a 200°C temper gives a hardness of 55. Optical micrographs of the undeformed microstructures are shown in Figures 1-3. For 1018 CRS, these reveal ferrite and pearlite; for HY-100, tempered martensite with large MnS inclusions. The AISI 4340 VAR steel also shows a tempered martensite microstructure, with the 425°C temper being considerably finer. The specimens used in this study were machined in the shape of thin-walled tubes with integral hexagonal flanges for gripping, Figure 4. Torsional loading at high strain rates was applied in a torsional Kolsky bar (split-Hopkinson bar), described by Costin et al. [4]. For present purposes, the torsional Kolsky bar is advantageous because it provides a relatively simple and uniform state of shear stress during dynamic deformation, because the instrumentation affords an easy means of measuring average strain as a function of time, and

because supplementary instrumentation can be added easily to measure local strain and the temperature distribution. Details are presented in reports on the individual steels, References [1,2,36]. It should be added, that to measure the local shear strain distribution along the thin-walled tubular specimen under dynamic loading, a grid of fine lines is deposited photographically on the outside surface of the specimen, Figure 4. Initially, the grids are oriented so the lines are parallel to the axis of the specimen. During the subsequent deformation the slope of the lines provides a measure of the strain distribution across the gage section. During deformation eight frames are recorded photographically at pre-set instants by means of a high-speed image-converter camera. These provide a time-history of the localization process. Alternatively, ultra-high speed flash photographs are made of the strain at various positions around the circumference of the specimen, to provide an understanding of shear banding as a function of distance.

2. Preparation of Specimens for Metallurgical Examination

The shear bands in the tubular specimens lie essentially in one plane, perpendicular to the axis of the specimen and generally near the center far from the shoulders. Shear bands have never been seen at either of the reentrant corners formed by the shoulders. Although all specimens develop a shear band in this test, a crack does not develop in all cases. When a crack does appear, it may follow the shear band only partly around the circumference of the specimen, or it may propagate completely around. As it turns out, the fact that we obtain both partial and complete fractures is convenient for the present microscopic observations. The completely fractured specimens are chosen for the fractography. But, to study incipient fracture, the specimens used are those in which a crack covered only a portion of the circumference. Under the latter conditions, the uncracked portion of the shear band shows a very high local strain. It should be remembered that the

magnitude of this local strain is known for each specimen from the slope of the grid lines deposited on the outer surface.

To prepare the specimens for observation, the uncracked wall section of the partially fractured specimens were cut with an electro-discharged machine (EDM) in order to reduce damage. The sectioned wall was then prepared for later metallurgical examination of the shear band material. Both optical and scanning electron microscopy (SEM) were employed. The microstructures of the shear bands were observed by optical microscopy after polishing and etching (nital). The specimens were also examined with SEM for microstructural defects, such as voids and microcracks within the shear band. SEM was also employed to observe the surface appearance of uncracked shear bands as well as the fracture surfaces of those specimens that had fractured.

C. Results and Discussion

1. Mechanical Behavior of the Three Steels Based on Results Obtained with the Kolsky Bar

The room temperature dynamic shear stress-strain curves of all three steels, as obtained with the torsional Kolsky bar, are shown in Figure 5. A general trend of the dynamic stress-strain behavior at room temperature is that a maximum shear stress is always reached, followed by a slight decrease in stress with further straining, and finally a rapid drop preceding fracture. The nominal strain at which the final rapid drop in stress occurs can vary from one test to another for a given steel. This was found to be influenced by geometric defects introduced during specimen preparation [36], consistent with the predictions of Molinari and Clifton [32]. The maximum shear strain at fracture in dynamic deformation, and the hardness of each of the three steels are given in Table 2. A more complete study of the mechanical behavior of the three steels under investigation can be found in the previously cited references [1,2,36].

Figures 6 and 7 are presented to illustrate the type of result that can be obtained by photographing the grid pattern on the specimen surface during deformation. Figure 6 shows changes in the slope of the grid lines at 40 microsecond intervals. The corresponding nominal strain values are identified on the stress-strain curve for the same test in Figure 7. The slopes of the grid lines provide the value of local strain. It appears from these that the strain distribution in this particular test remains homogeneous until a strain of about 20 or 25% has accumulated. Shear banding seems to start in the fifth frame (γ_{nom} = 33%) and be well underway by the sixth (γ_{nom} = 38%). Beyond that, the specimen has probably fractured or, at least, a macrocrack has appeared at the observed location. Clearly, more detail is necessary and this is provided with the same high speed camera by reducing interframe time. For instance, a ten microsecond interframe time can be used to study in more detail the evolution of the shear band in the region of the knee in the stress-strain curve, where the stress starts to drop more sharply. An alternative method of photographic observation is to take simultaneous ultra-high speed flash photographs at various points on the specimen's circumference. By this means, it has been shown that the maximum local strain need not be the same at all points on the circumference [1]. There can be large differences in local strain, particularly starting at the knee in the stress-strain curve and through the large stress drop. For more details, the reader is referred to previous publications [1,2]..

2. Microscopic Observations of Shear Bands

2-1. AISI 1018 Cold-Rolled Steel

Figure 8 is an optical micrograph of the shear band formed in AISI 1018 CRS. The horizontal direction in the photograph, i.e. the direction of the shear band, is perpendicular to the axis of the specimen and to the direction of rolling of the original steel. As was seen in Figure 1, the rolling process elongated and crushed the ferrite and pearlite grains. These grains are further elongated as a result of shear banding. Indeed, the slope of the grains could be used as a measure of the strain, as pointed out by Moss [37]. Similar effects have been seen previously, as for instance by Rogers [38], as well as in the machining experiments of Semiatin et al. [39].

In addition to the shear band, the photograph reveals a fine crack that arrested after running near the center of the shear band. Examination of the fracture surface of this crack reveals it propagated in a ductile manner, see Section 3. The average local shear strain γ_{loc} is about 600%, and the average width w of the shear band is about 100μm. By measuring the infrared radiation emanating from the metal surface, it has been shown that the maximum temperature rise in the shear band is about 450°C [2]. Microscopic observation shows the shear band to be characteristic of a deformed band: it does not etch white and is fairly wide, Figure 8. However, the temperature rise, undoubtedly contributes to the enhancement of the local shear deformation.

SEM was used for more detailed observations of specific areas in Figure 10. These are identified as A, B and C in the figure and shown in Figures 9 and 10. Of these, the area A was chosen to be near the center of the crack, B near one end, and C within the shear band, but about 150μm beyond the tip of the crack. These figures reveal the presence of voids and microcracks inside the shear band. Most of these voids are elongated and have some inclination to the direction of the shear band (marked with arrows). Coalescence and linkage of these voids and microcracks

lead to the crack shown in Figure 8 and, with continued straining, to complete fracture.

In order to investigate possible initiation sites of voids and microcracks, the polished specimens shown in Figure 9 were etched with nital, Figure 12. Comparison of Figures 9 and 10, reveals that the voids and microcracks initiate through one of the following mechanisms:

(1) by decohesion of the interface between ferrite and pearlite;

(2) by the breaking apart of a single long pearlite lamella; or

(3) by the separation of ferrite grain boundaries, possibly due to the cracking of the precipitated carbide layers shown in Figure 1.

Of these, the dominant mechanisms are (1) and (2), although each of these two probably requires a different level of local strain. As may be seen in Figure 9(c) the spacing between the arrays of the elongated voids is of comparable magnitude with the distance between pearlite lamellae within the shear band. In high temperature deformation, the grain boundaries and interfaces generally become weaker than the slip planes within the grains. For example, intergranular cracking is frequently seen as a result of hot-working [40]. Since the temperature within the shear band is rising during deformation, the decohesion of the ferrite-pearlite interfaces and the separation of ferrite grain boundaries become easier. Thus mechanisms (1) and (3) become more significant because of the higher temperatures, although the fracture of pearlite lamellae remains an important mechanism. At this stage, fracture of the pearlite lamellae is influenced more by the localized strain within the shear band (about 600% on the average) than by thermal effects.

2.2. HY-100 Structural Steel

The microstructure of the shear band formed in an HY-100 steel during dynamic torsional testing is shown in Figure 11. It should be remembered that this steel has about the same degree of ductility as does CRS, Figure 5. The flow of the material

within the shear band is quite evident in the figure, even though no clear marks exist. such as the highly elongated grains observed in CRS. Voids and linked voids are also shown at several locations near the center-line of the shear band. The maximum local shear strain in the figure shown is about 1000% and the average width of the shear band is about 20μm.

In a previous investigation [2], the maximum local strain measured in this steel was about 1900%. The maximum recorded temperature was 590°C. However, based on the fact that the shear band was narrower than the area observed by the infra-red detectors, it was estimated that the peak temperature at the center of the shear band was about 1140°C. The general appearance of shear bands in this steel is shown in Figure 11 (a), which shows a white etched region in the center of the shear band and deformed features on the edges, Figure 11(b). Figure 12 (a) is an optical micrograph of the shear band in HY-100 steel obtained by means of a polarized light. It may be noted that the shear band in CRS does not reveal white etched area under polarized light implying that no phase transformation occurred in this steel. SEM micrography of the shear band in HY-100 before polishing and etching is shown in Figure 12 (b), which provides evidence of ductile flow lines in the material. As shown in Figure 2, HY-100 steel contains manganese sulfide (MnS) inclusions. These are relatively large and may be either in the form of globules or stringers. During deformation, voids will initiate at either form of inclusion. Figure 11(b) is a magnified view of the area indicated by A in Figure 11(a). It shows voids within the shear band formed at globular MnS inclusions and connected with one another. In Figure 13(a), SEM is used to show voids formed inside the shear band by MnS stringers, (a few globular voids are also seen). The linkage of voids formed at globular MnS inclusions is shown in Figure 13(b). With higher magnification, the fragments of a MnS stringer can be seen inside a void, Figure 13(c). Identification is effected by means of EDAX, Figure 13(d). Voids can initiate

by fracture of MnS stringers or by decohesion at the interfaces between the matrix and the MnS inclusions. Since the temperature rise within the shear band is quite high, one can expect ductile deformation of the material due to thermal softening. As will be seen later, highly elongated ductile dimples on the fracture surface provide evidence of this ductile deformation. With continued deformation, the decohesion of the MnS/matrix interface occurs more easily under the combination of the temperature effect and of the increasing stress along the interface.

2-3. AISI 4340 Vacuum Arc Remelted Steel

This section presents the results of microscopic examinations of the shear bands in the two tempers of the AISI 4340 VAR steel. Their microstructures were shown previously, Figure 3, although a more complete description is given in Reference [35], in which it is shown that shear bands will form with either microstructure. Optical micrographs of the shear bands after polishing and etching in nital are shown in Figure 14(a). The shear band in the 200°C temper (RHC = 55) reveals a white etched band with sharp edges, indicating that this is a transformed band. As may be seen in Figure 14 (c), observation of the shear band in polarized light accentuates the difference between shear material and the matrix. SEM micrography, Figure 15(a) shows the sharp edges separating the shear band and the matrix, and the different features in each. In addition to etching white, further evidence of a phase transformation is provided by the fact that the bands have distinct boundaries and a well-defined width [24]. The width of the shear bands we observed in steels of this temper lies in the range of 2μm to 5μm, with a maximum local shear strain of about 2000%.

Shear bands in the 425°C temper (RHC = 44) were also examined using optical microscopy, Figure 14(b), polarized light microscopy, Figure 14 (d), and SEM, Figure 15(b). Both provide micrographs strongly characteristic of a transformation band, i.e, the shear band area is white after etching and its edges are relatively

well-defined with different surface features apparent within the shear band area and the matrix. However, some characteristics of a deformed band can be seen in the 425°C temper. The plastic flow lines of the material are quite apparent just outside the shear band, contrasting with the transformed area where flow lines are more difficult to see although the deformed grid pattern shows that large shear strain has occurred. One should note that flow lines outside the shear band are nearly completely absent in the 200°C temper, i.e. this shows none of the characteristics of a deformed band. For the 425°C temper, the average width of the shear band is approximately 10μm, and the maximum local shear strain is about 1500%.

3. Fractography

The intensely localized deformation constituting a shear band frequently leads to fracture of the specimen. In the four microstructures tested and for the strain rates imposed, fracture always proceeds through the growth and linkage of voids and microcracks along the shear band. Although, as will be seen, the appearance of the fracture surface depends strongly on the particular steel tested, no cleavage facets or other evidence of brittle fracture was observed for any of the four steels. At first sight, this seems a surprising result, particularly in the case of the 4340 VAR steel hardened to RHC 55. That steel shows narrow shear bands of the transformed type with hardly any evidence of a deformed band or of higher local strains to either side of the shear band. Since the transformed material is known to be highly brittle and since fracture in this steel occurs suddenly under present test conditions, i.e. with almost no additional strain once fracture initiates, one might expect a brittle fracture. It is clear, however, that the fracture process is ductile, and therefore, probably occurs when the metal is hot. Thus, the most distinctive feature of the fracture surfaces in the present dynamic shear tests is the fibrous nature of the fracture. This is indicated by the presence of highly elongated dimples. Another

feature characteristic of certain areas of the fracture surfaces is a smoothed and smeared appearance of the surface, produced probably by the rubbing of opposing fracture surfaces and perhaps by the frictional heating following fracture. These two features were seen in all four microstructures investigated.

3.1 AISI 1018 Cold-Rolled Steel

Figure 16 presents typical SEM fractographs of areas of the fracture surface of the AISI 1018 CRS. The fracture surface is made up of regions of highly elongated dimples, Figure 16(a), and regions with a smoothed and smeared appearance, as shown in Figure 16(b). A transition from a dimpled fracture to a smooth surface is also observed. The origin of the elongated dimples probably lies in the voids which were found within the shear band, Figures 9 and 10. Some evidence of a knobbly fracture surface, which is most frequently observed in aluminum alloys, is also found. As a possible mechanism to explain this knobbly appearance, Rogers proposed a thermal alteration of the surface in certain areas occurring as a result of the frictional heat generated when the two fracture surfaces rub one another [24]. Small patches of knobbly-like features are seen at several locations in Figure 16(a). These could be formed through the mechanism proposed by Rogers.

3.2 HY-100 Structural Steel

The fracture surface of HY-100 steel specimens, Figure 17, shows highly elongated dimples oriented in the direction of shearing, indicating ductile fracture, Figure 17(a). Again, one sees smoothed and smeared surface areas probably due to rubbing of opposing fracture surfaces, Figure 17(b). Some evidence of a knobbly-like fracture is also shown. Figures 17(a) shows a large-sized dimple. Many of these large dimples contain pieces of broken MnS stringers, suggesting that MnS provides the initiation sites for the voids. This would be consistent with the role of MnS

during void formation in shear bands as described in the preceeding section, Figures 15 and 16. The globular MnS, which also provides initiation sites for voids, is believed buried within smaller sized dimples.

3.3 AISI 4340 VAR Steel

Representative fracture surfaces of two different microstructures of the AISI 4340-VAR are shown in Figures 18 and 19. In addition to the features typical of fracture surfaces in shear bands i.e., ductile dimples and smoothed and smeared surface areas, it is also possible to see the knobbly-like fracture at the boundaries between dimpled and smeared areas. A typical knobbly-like fracture surface is shown in Figure 19(c) for the 425°C temper. The smeared surface area can be seen on the right of the photograph.

Two different dimples sizes are observed on the fracture surfaces of the 200°C temper steel as well as on the 425°C temper. During fracture in these two steels the crack appears to follow the shear band, at least for the most part, as it propagates around the circumference of the specimen. However, it must be remembered that the shear band is very narrow in these steels. It is supposed, therefore, that occasionally the crack path moves out of the plane of the shear band. Whether this occurs because the shear band does not lie precisely within one plane or because the crack path is not planar, or both, is not clear. Whatever the reason, a typical fracture surface in the 200°C temper steel, Figure 18(a), shows a fairly large patch in which the crack was probably just outside the plane of the shear band. This patch is quite wide, since it goes almost all the way across the wall-thickness of the specimen. Small dimples, less than 1 μm, are dominant over the main fracture surface, i.e. the surface lying within the shear band. In the patch, however, the dimples are larger, measuring 2 or 3μm across. A similar situation obtains in the 425°C temper, Figure 19. Here, the larger dimples outside the plane of the shear band, Figure 19(a),

measure 3 to 5μm, while those within the shear band average about 1μm across. It is generally believed that second phase particles, for example carbide particles in the 4340 VAR steel [35], provide nucleation sites for voids. In a plastically deforming material, voids generally form first at the larger particles. But with the higher plastic strains that occur during the later stages of deformation, voids also can initiate at smaller particles. Therefore, the smaller dimples, shown in Figures 18(c) and 19(b), may be formed when the crack lies within the shear band at smaller particles and under higher local strains. The large dimples, however, occur when the crack lies in the less highly deformed region outside the shear band. Since there is less strain in the region outside the shear band, the voids will form mainly around larger particles.

For all four microstructures in the present study the fractography suggests that the fracture process following shear localization may be strongly affected by heating due to the temperature rise within the shear band. The evidence for this lies in the elongated dimples which indicate a ductile mode of fracture in dynamic shear deformation. The appearance of the smoothed and smeared surface and the knobbly-like features are probably due to a sequence of ductile deformation and frictional heat generated by rubbing of opposing fracture surfaces.

D. Conclusions

Microscopic observations were made of the shear band material in three different steels. In all cases the shear bands were produced by the dynamic torsional deformation of thin-walled tubular specimens. Failure, i.e. an essentially complete loss in the load carrying capacity does not always involve fracture. When fracture is involved, the observations show voids and microcracks leading eventually to fracture. Even for the most brittle steel tested no cleavage was observed on any fracture surface, presumably because of the large local temperature rise. At the strain

rates imposed in the present experiments, the shear bands in AISI 1018 CRS are of the deformed type. In this steel, microcracks initiate by the decohesion of phase boundaries between the ferrite and pearlite, by the fracture of pearlite and possibly by the separation of ferrite grain boundaries where precipitation of a carbide film has occurred. Fracture is completed by the linkage of the microcracks to one another within the shear band. HY-100 steel forms deformed bands mostly but some evidence of a phase transformation within the deformed band is observed as well. Manganese sulfide which exists in the form of stringers and globular particles provides initiation sites for voids, or microcracks within the shear bands. Coalescence of these voids precedes the final fracture. AISI 4340 VAR steel is a relatively clean steel with a uniformly tempered martensitic microstructure that shows little evidence of inhomogeneities, such as those found in 1018 CRS or in the HY-100 steel. Fine carbide particles in the tempered martensite for both 200°C and 425°C tempers probably serve as the nucleation sites of the voids. The small size of the dimples on the fracture surfaces are evidence that the voids form at the carbide particles. The shear bands observed in both tempers of AISI 4340 VAR steel are of the transformed type.

Recent modeling of shear bands has shown that dimensional variations or temperature variations will trigger shear bands [32,33]. This modeling has shown that the same metal under similar deformation conditions will show shear banding at a lower value of strain for larger dimensional or temperature defects. Experimental evidence is in agreement with these results [36]. It seems likely that a similar effect can be produced by the second phase particles, inclusions, etc., which constitute microstructural defects. While these may be more difficult to relate quantitatively to shear banding than, for instance, a dimensional variation, they are nevertheless of considerable practical significance. It is clear, therefore, that future tests should be

performed with more controlled microstructures, e.g. microstructures with different size, shape or density of inclusions.

Acknowledgements

The authors wish to acknowledge the research support of the Army Research Office under Grant No. DAAL03-88-K-0015 and the NSF Materials Research Laboratory at Brown University. The authors also thank Mr. George LaBonte for his help in the experiments.

References

1. A. Marchand and J. Duffy, "An Experimental Study of the Formation Process of Adiabatic Shear Bands in a Structural Steel", J. Mech. Phys. Solids, Vol. 36, 1988, pp. 251-283.

2. K.A. Hartley, J. Duffy and R.H. Hawley, "Measurement of the Temperature Profile during Shear Band Formation in Steels Deforming at High Strain Rates", J. Mech. Phys. Solids, Vol. 35, 1987, pp. 283-301.

3. J. Duffy, "Temperature Measurements during the Formation of Shear Bands in a Structural Steel", in Mechanics of Material Behavior, ed. by G.J. Dvorak and R.T. Shield, Elsevier, Amsterdam, 1984, pp. 75-86.

4. L.S. Costin, E.E. Crisman, R.H. Hawley and J. Duffy, "On the Localization of Plastic Flow in Mild Steel Tubes under Dynamic Torsional Loading", 2nd Conf. on Mechanical Properties of Materials at High Rates of Strain, ed. by J. Harding, The Institute of Physics, London, 1979, pp. 90-100.

5. S.P. Timothy and I.M. Hutchings, "The Structure of Adiabatic Shear Bands in a Titanium Alloy", Acta Met., Vol. 33, 1985, pp. 667-676.

6. S.P. Timothy and I.M. Hutchings, "Initiation and Growth of Microfractures along Adiabatic Shear Bands in Ti-6Al-4V", Mat. Sci. Tech., Vol. 1, 1985, pp. 526-530.

7. H.A. Grebe, H. Pak and M.A. Meyers, "Adiabatic Shear Localization in Titanium and Ti-6Pct Al-4Pct V Alloy", Metal. Trans., Vol. 16A, 1985, pp. 761-775.

8. R.E. Winter, "Adiabatic Shear of Titanium and Polymethylmethacrylate", Philos. Mag., Vol. 31, 1975, pp. 765-773.

9. P.W. Leech, "Observations of Adiabatic Shear Band Formation in 7039 Aluminum Alloy", Metal. Trans. Vol. 16A, 1985, pp. 1900-1903.

10. A.L. Wingrove, "The Influence of Projectile Geometry on Adiabatic Shear and Target Failure", Metall. Trans., Vol. 4, 1973, pp. 1829-1833.

11. T.C.A. Stock and K.R.L. Thompson, "Penetration of Aluminum Alloys by Projectiles", Metall. Trans., Vol. 1, 1970, pp. 219-224.

12. M. Hartherly and A.S. Malin, "Shear Bands in Deformed Metals", Scripta Met., Vol. 18, 1984, pp. 449-454.

13. T. Quadir and P.G. Shewmon, "Solid Particle Erosion Mechanisms in Copper and Copper Alloys", Metall. Trans., Vol. 12A, 1981, pp. 1163 - 1176.

14. J.V. Craig and T.A.C. Stock, "Microstructural Damage Adjacent to Bullet Holes in 70-30 Brass", J. Aust. Inst. Met., Vol. 15, 1970, pp. 1-5.

15. J.H. Giovanola, "Adiabatic Shear Banding under Pure Shear Loading. - Part II: Fractographic and Metallographic Observations," to be published in Mechanics of Materials.

16. M. Azrin, J.G. Cowie and G.B. Olson, "Shear Instability Mechanisms in High Hardness Steel", U.S. Army Materials Technology Laboratory Report No. MTL TR 87-2.

17. H. Yaguchi, K.A. Hartley, J. Duffy and R.H. Hawley, "The Effect of MnS Inclusions in AISI 1215 Free-Machining Steels on Shear Band Formation during High Strain Rate Torsional Deformation", Proc. 2nd Int. Symp. on The Effects and Control of Inclusions and Residuals in Steels, Toronto, Canada, 1986 pp. 68-82.

18. R.L. Woodward and R.L. Aghan, "The Structure of a White-Etching Band in an Explosively Fractured Steel", Metal Forum, Vol. 1, 1978, pp. 180-184.

19. R. Dormeval and M. Stelly, "Study of Adiabatic Shear Bands by Means of Dynamic Compressive Test", 7th Int. Conf. on High Energy Rate Fabrication, The University of Leeds, 1981.

20. H.C. Rogers and C.V. Shastry, "Materials Factors in Adiabatic Shearing in Steels", in Shock Waves and High Strain Rate Phenomena in Metals, ed. by M.A. Meyers and L.E. Murr, Plenum Press, New York, 1981, pp. 285-298.

21. P.A. Thornton and F.A. Heiser, "Observations on Adiabatic Shear Zones in Explosive Loaded Thick-Wall Cylinders", Metall. Trans., Vol. 2, 1971, pp. 1496-1501.

22. R.C. Glen and W.C. Leslie, "The Nature of White Streaks in Impacted Steel Armor Plate", Metall. Trans. Vol. 2, 1971, pp. 2945-2947.

23. A.S. Argon, "Stability of Plastic Deformation", in The Inhomogeneity of Plastic Deformation, Chap. 7, American Society for Metals, Metal Park, OH, 1973, pp. 161-189.

24. H.C. Rogers, "Adiabatic Plastic Deformation", Ann. Rev. Mat. Sci., Vol. 9, 1979, pp. 283-311.

25. H.C. Rogers, "Adiabatic Shearing: A Review", Drexel University Report for U.S. Army Research Office, 1974.

26. A.J. Bedford, A.L. Wingrove and K.R.L. Thompson, "Phenomenon of Adiabatic Shear Deformation", J. Aust. Inst. Metals, Vol. 19, 1974, pp. 61-73.

27. R.J. Clifton, "Adiabatic Shear Banding" in Material Response to Ultra High Loading Rates, Chap. 8, National Materials Advisory Board Committee, Report No. NMAB-356, 1980, pp. 129-142.

28. G.B. Olson, J.F. Mescall and M. Azrin, "Adiabatic Deformation and Shear Localization", in Shock Waves and High Strain Rate Phenomena in Metals, ed. by M.A. Meyers and L.E. Murr, Plenum Press, New York, 1981, pp. 221-247.

29. J.W. Hutchinson, View Point Set No. 6, Scripta Met., Vol. 18, 1984, pp. 421-458.

30. S.P. Timothy, "The Structure of Adiabatic Shear Bands in Metals: A Critical Review", Acta Met., Vol. 35, 1987. pp. 301-306.

31. M.E. Backman and S.A. Finnegan, "The Propagation of Adiabatic Shear" in Metallurgical Effects at High Strain Rates, Ed. by R.W. Rohde, B.M. Butcher, J.R. Holland and C.H. Karnes, Plenum Press, New York 1973, pp. 531-543.

32. A. Molinari and R.J. Clifton, "Analytical Characterization of Shear Localization in Thermoviscoplastic Materials", J. Appl. Mech., Vol. 5, 1987, pp. 806-812.

33. T.W. Wright and J.W. Walter, "On Stress Collapse in Adiabatic Shear Bands," J. Mech. Phys. Solids, Vol. 35, 1987, pp. 701-720.

34. T.J. Baker and J.A. Charles, "Deformation of MnS Inclusions in Steel", J. Iron and Steel Inst., 1972, pp. 680-690.

35. Y.C. Chi, S.H. Lee, K. Cho and J. Duffy, "The Effects of Tempering and Test Temperatures on the Dynamic Fracture Initiation Behavior of an AISI 4340 VAR Steel," Brown University Technical Report, August, 1988.

36. Y.C. Chi and J. Duffy, unpublishd results.

37. G.L. Moss, "Shear Strains, Strain Rates and Temperature Changes in Adiabatic Shear Bands," Chapter 19 in Shock Waves and High-Strain-Rate Phenomena in Metals, ed. by M.A. Meyers and L.E. Murr, Plenum Press, 1981, pp. 299-312.

38. H.C. Rogers, "Adiabatic Shearing - General Nature and Material Aspects", in Material Behavior under High Stress and Ultrahigh Loading Rates ed. by J. Mescall and V. Weiss, Plenum Press, 1982, pp. 101-118.

39. S.L. Semiatin, G.D. Lahoti, and S.I. Oh, "The Occurrence of Shear Bands in Metalworking," in Material Behavior under High Stress and Ultrahigh Loading Rates ed. by J. Mescall and V. Weiss, Plenum Press, 1982, pp. 119-159.

40. J. Gurland and J. Plateau, "The Mechanism of Ductile Rupture of Metals Containing Inclusions," Trans. ASM, Vol. 56, 1963, pp. 442-454

D:Chorefs.wp
8/23/88
lmp

Table 1. Chemical Compositions (Wt %)

(a) 1018 CRS Steel

C	Mn	P	S
.18	.71	.020	.022

(b) HY-100 Steel

C	Mn	P	S	Si	Ni	Cr	Mo	Pb
.19	.29	.006	.014	.23	2.56	1.68	.45	.013

(c) 4340 VAR Steel

C	Mn	P	S	Si	Ni	Cr	Mo	Cu	Al	N	O
.42	.46	.009	.001	.28	1.74	.89	.21	.19	.031	.005	.001

*H(ppm):1.0

Table 2. Results of shear localization in the dynamic torsional tests. [1, 2, 36]

	1018CRS	HY-100	4340VAR 200 Temp.	4340VAR 425 Temp.
$Max(\gamma)_{nom}$	50%	50%	15%	20%
$Max(\gamma)_{loc}$	600%	1000%	2000%	1500%
$\dot{\gamma}_{nom}$	1000/s	1000/s	1000/s	1000/s
HRC	60(HRB)	26	55	44
w_{avg}	100μm	20μm	2-5μm	10μm

(a)

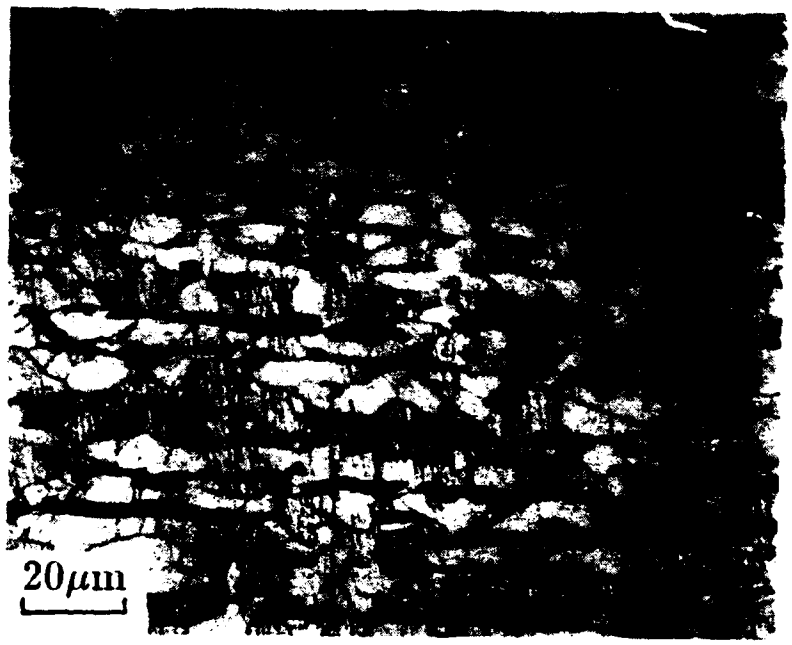

(b)

Figure 1. Optical micrographs of 1018 CRS before testing. The arrow indicates the rolling direction of the steel bar. (a) The elongated grains of the ferrite (white) and pearlite (dark). (b) Higher magnification reveals the precipitation of a carbide film between the ferrite grains (arrows).

(a)

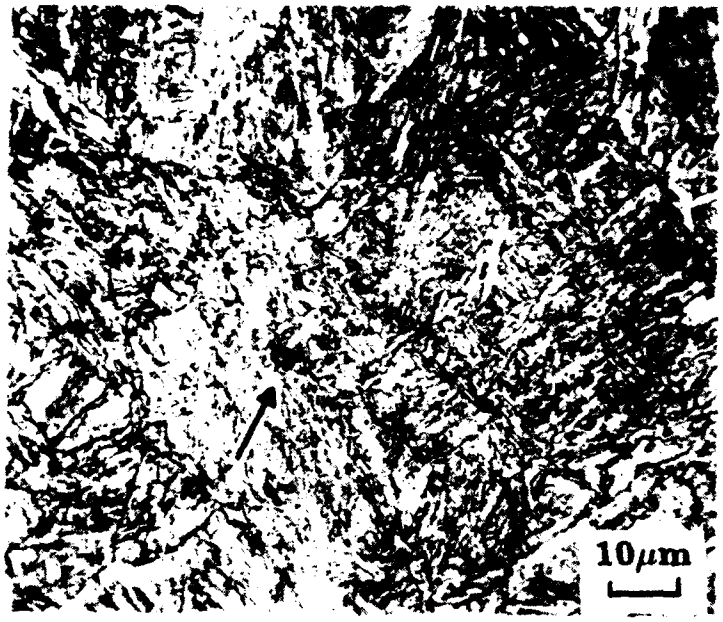

(b)

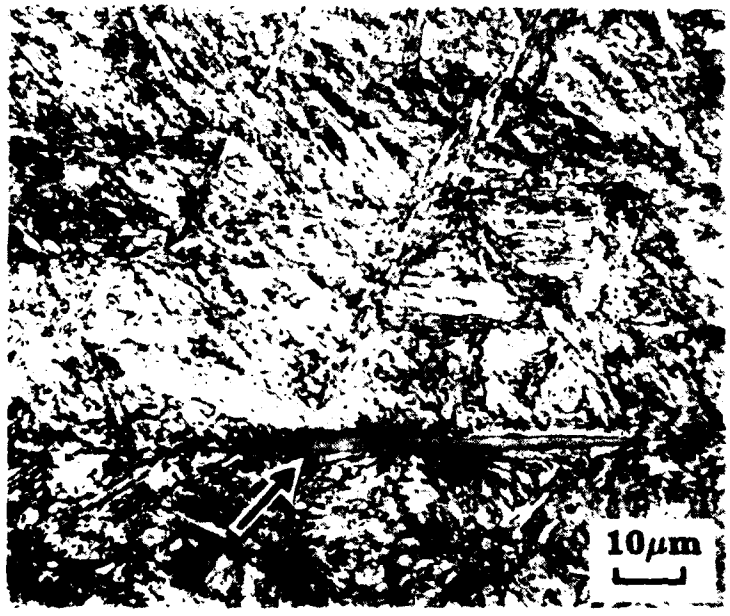

Figure 2. Optical micrographs of undeformed HY-100 steel showing a tempered martensitic microstructure containing MnS inclusions in the form of (a) a globule and (b) a stringer, indicated by arrows.

(a)

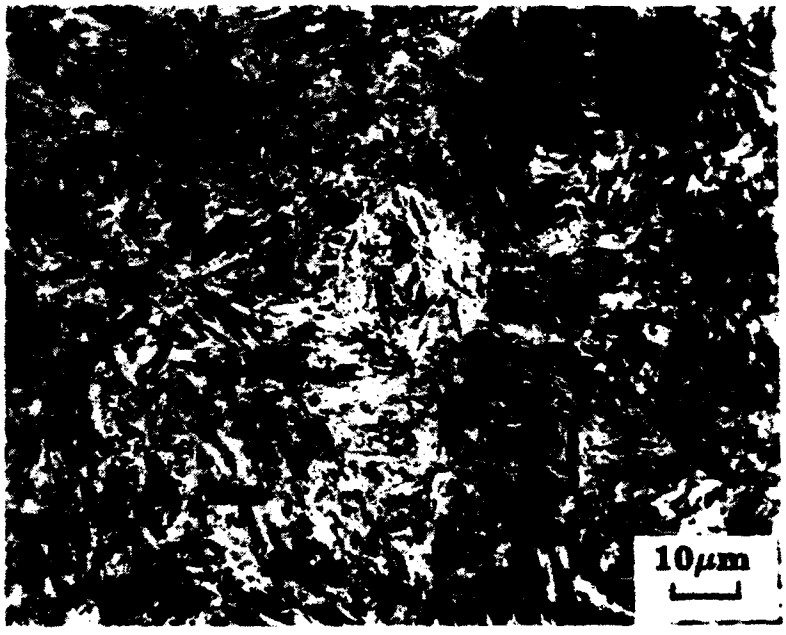

(b)

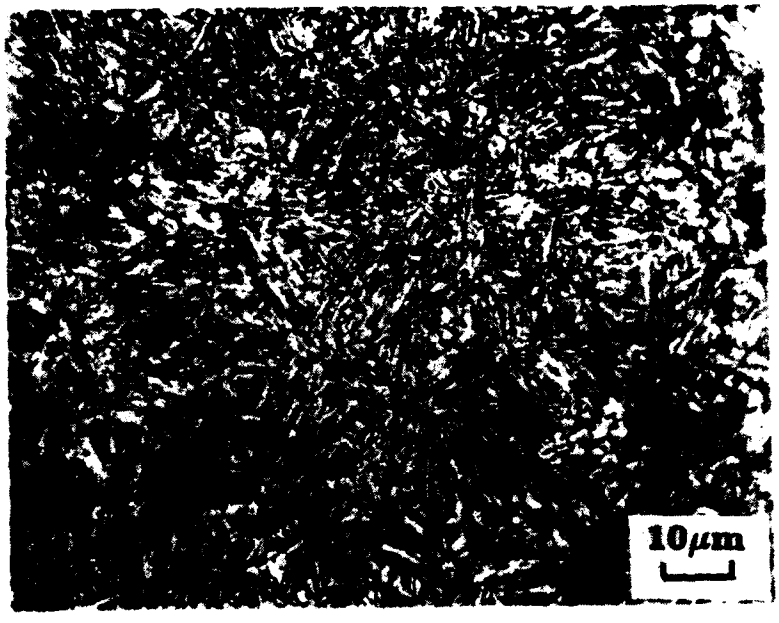

Figure 3. Optical micrographs of undeformed 4340 VAR steel. (a) Tempered at 200 C to RHC 55 and (b) tempered 425 C to RHC 44. A tempered martensitic microstructure may be seen, with a considerably finer morphology for the 425 C temper.

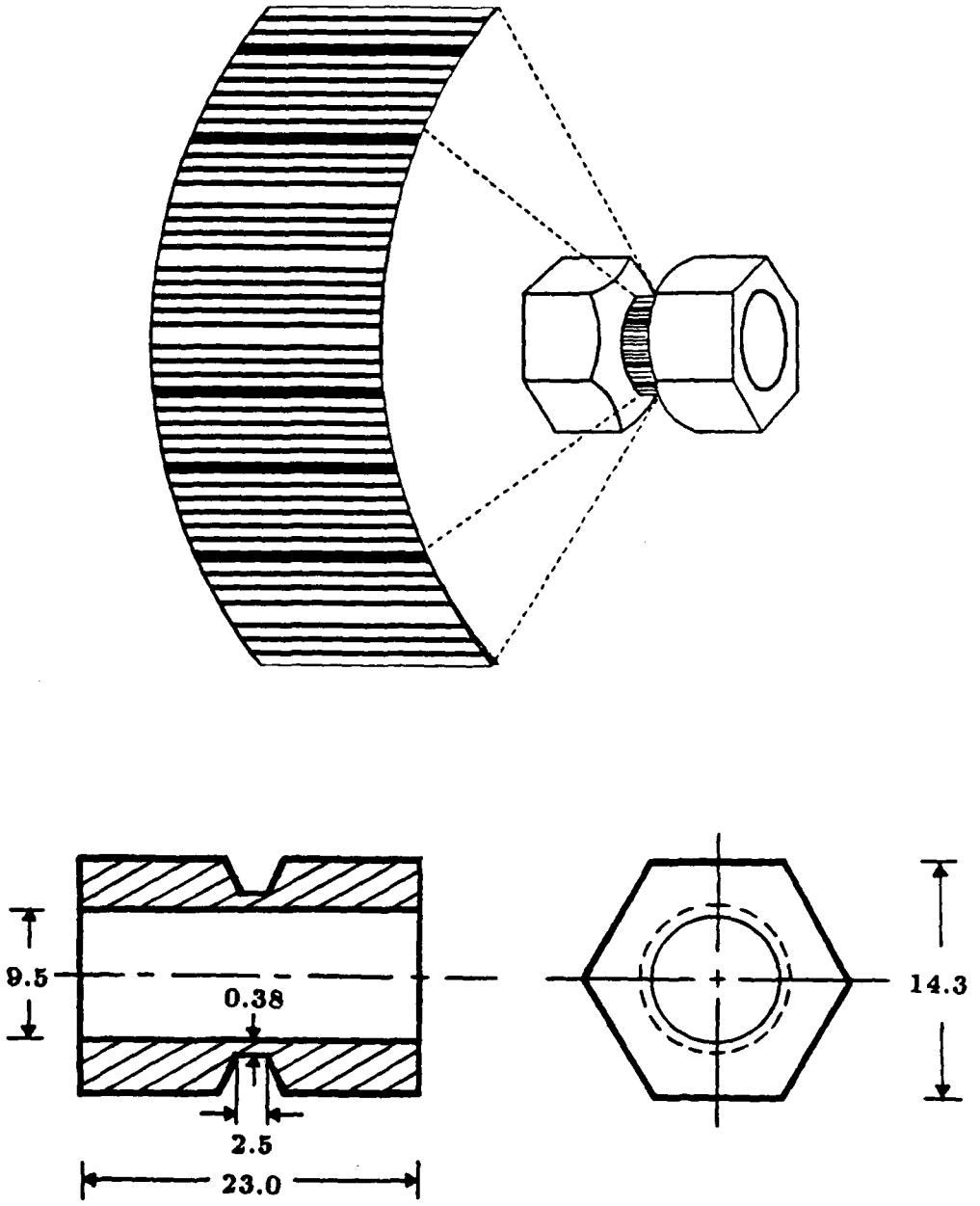

Figure 4. Details of the thin-walled tubular specimen with a blow-up of the fine grid deposited photographically on the outside surface of the specimen. The dimensions are in milimeters.

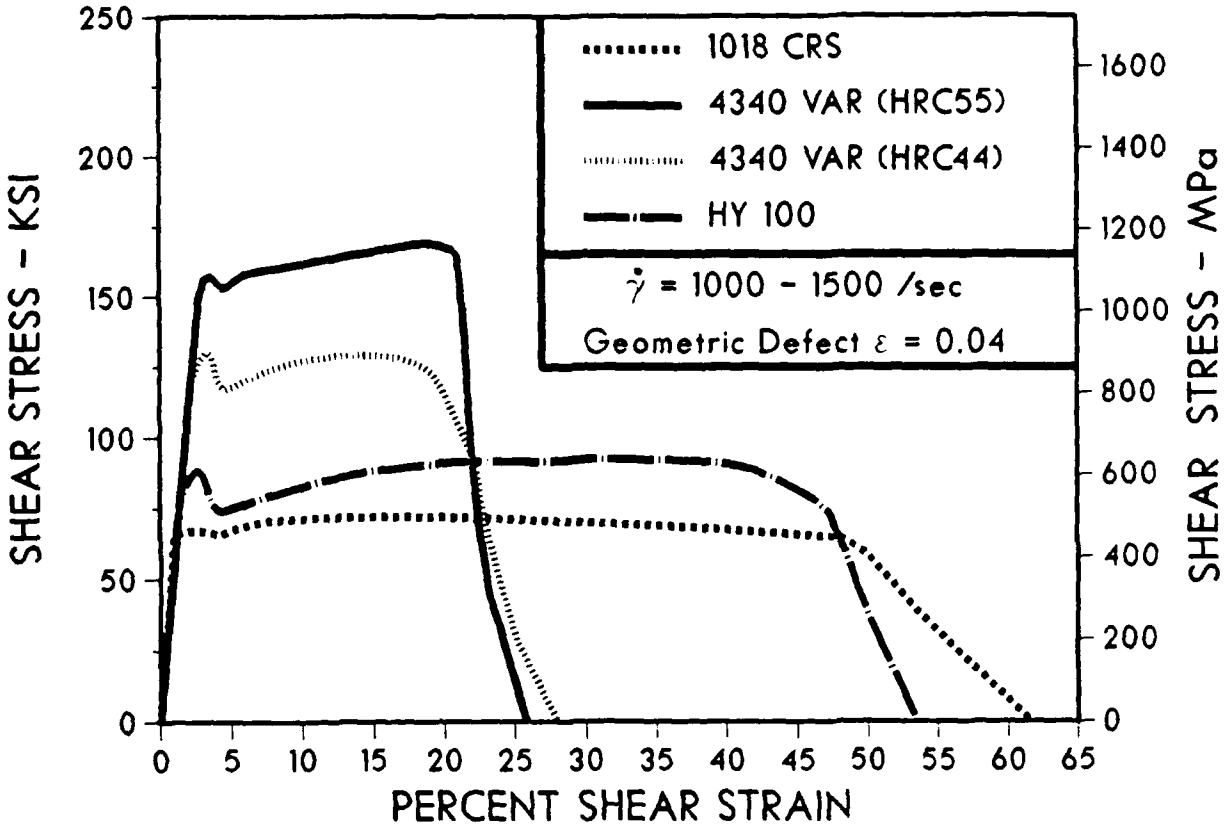

Figure 5. Typical stress-strain curves at a strain rate of $10^3/s$ for each of the four steels tested with the torsional Kolsky bar.

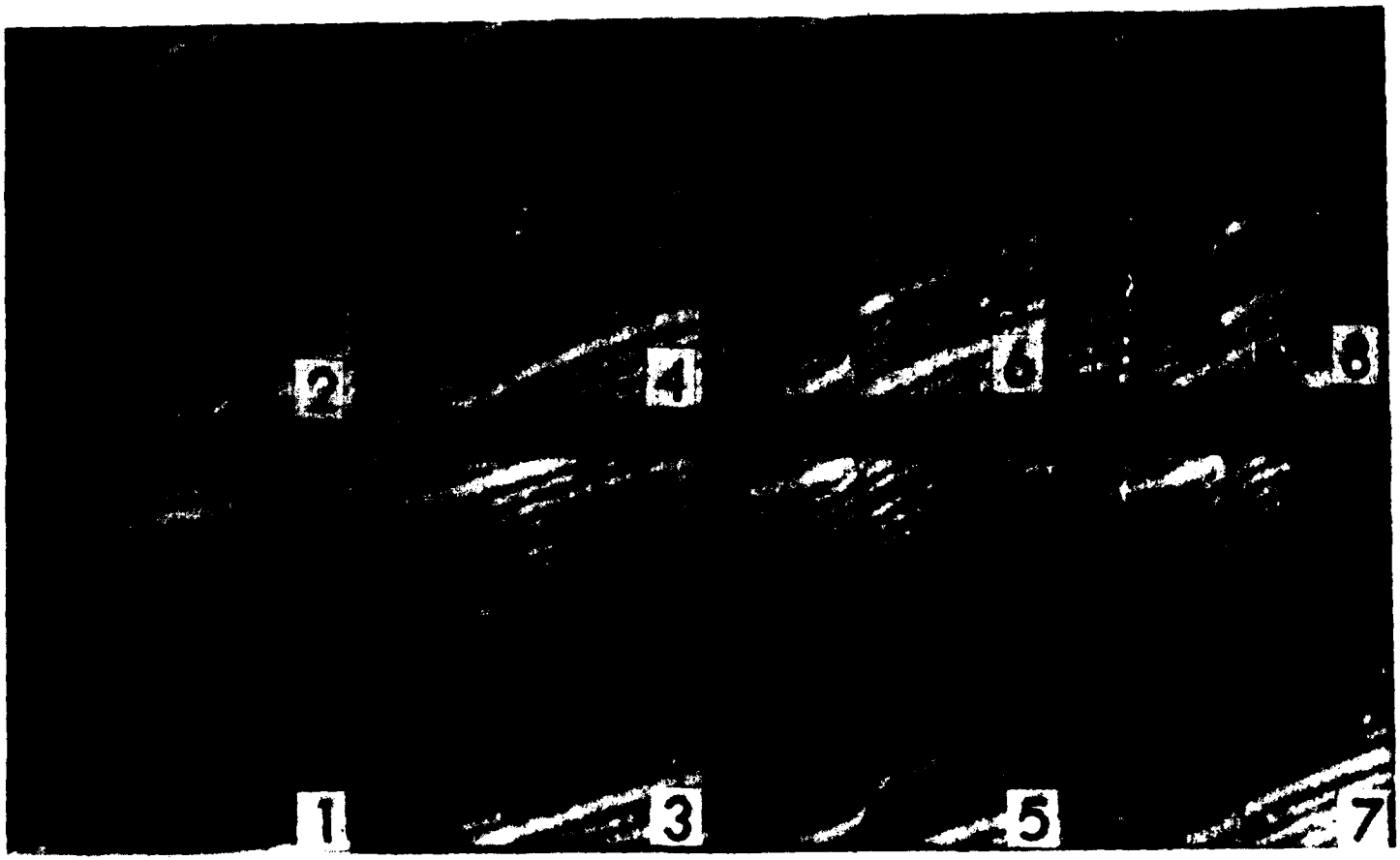

Figure 6. Photographs of the grid pattern during the formation of a shear band in HY-100 steel taken by a high speed image converter camera. The time interval between frames is 40μsec.

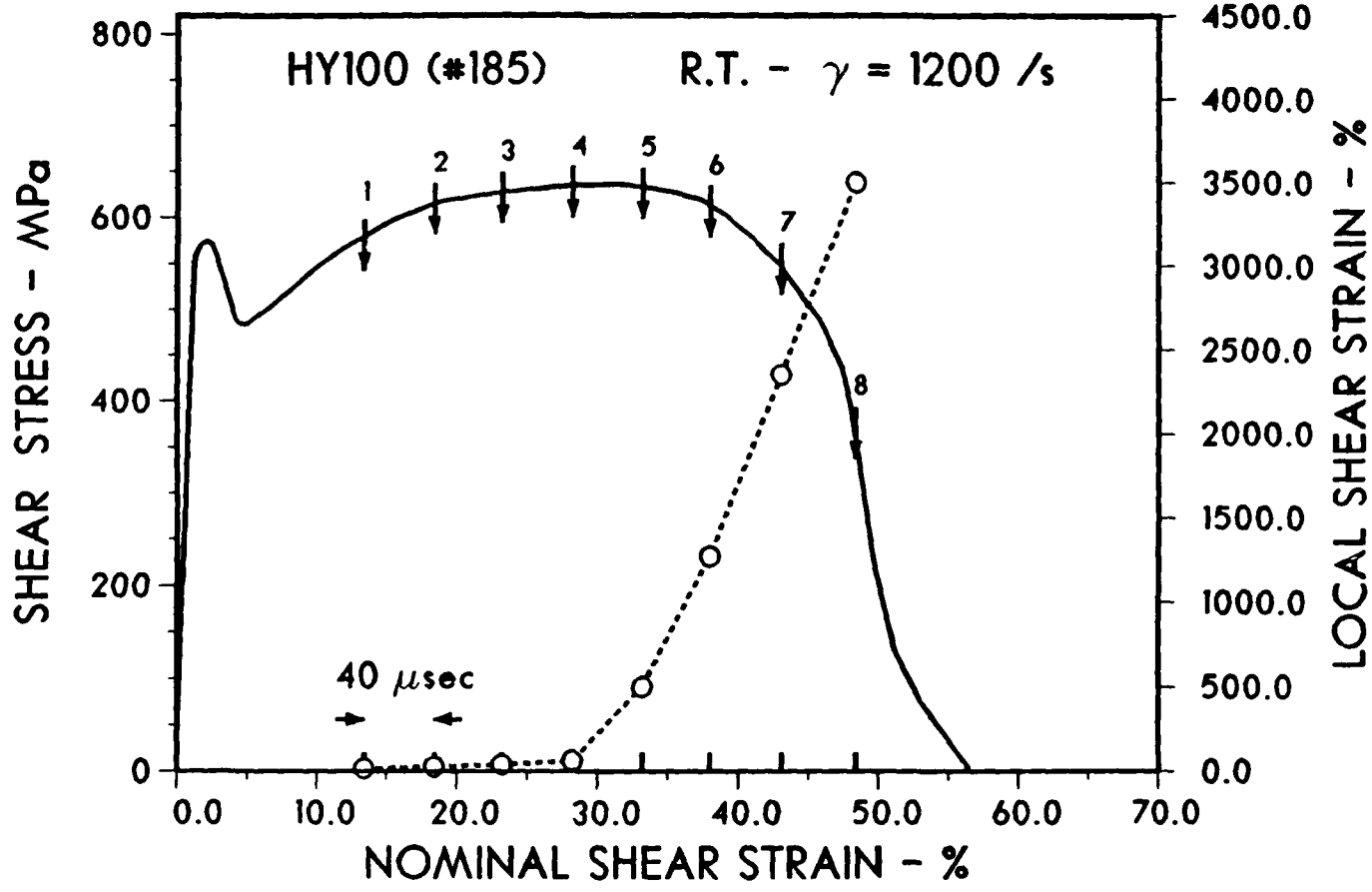

Figure 7. The stress-strain behavior of HY-100 steel. The numbered arrows indicate nominal strain values at which the photographs shown in Figure 6 are taken. The corresponding values of the maximum local strain are shown by the dotted line.

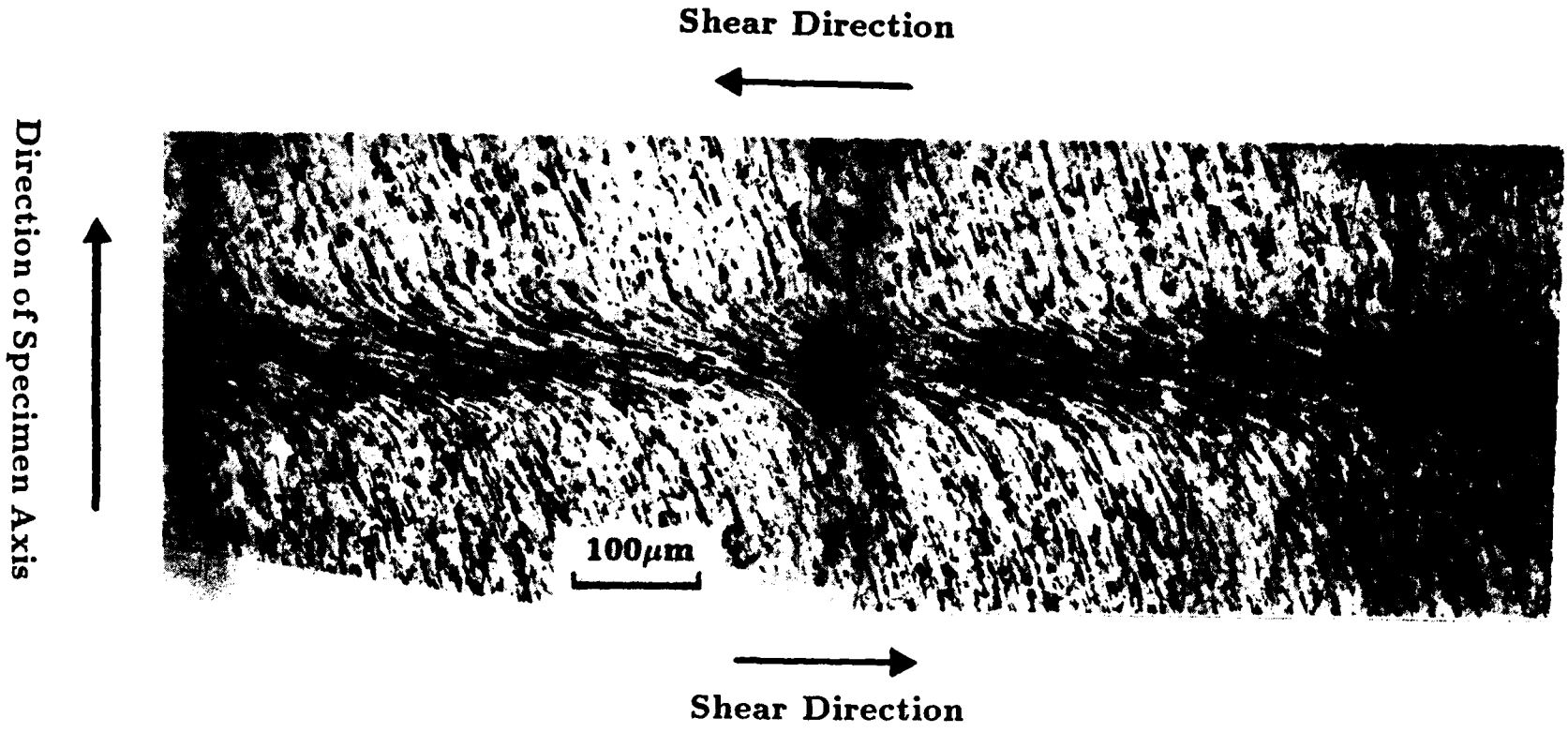

Figure 8. An optical micrograph of a shear band formed in 1018 CRS. The surface has been polished and etched. An arrested crack is shown within the shear band. Letters A, B and C refer to areas shown in greater detail in Figures 9 and 10.

(a)

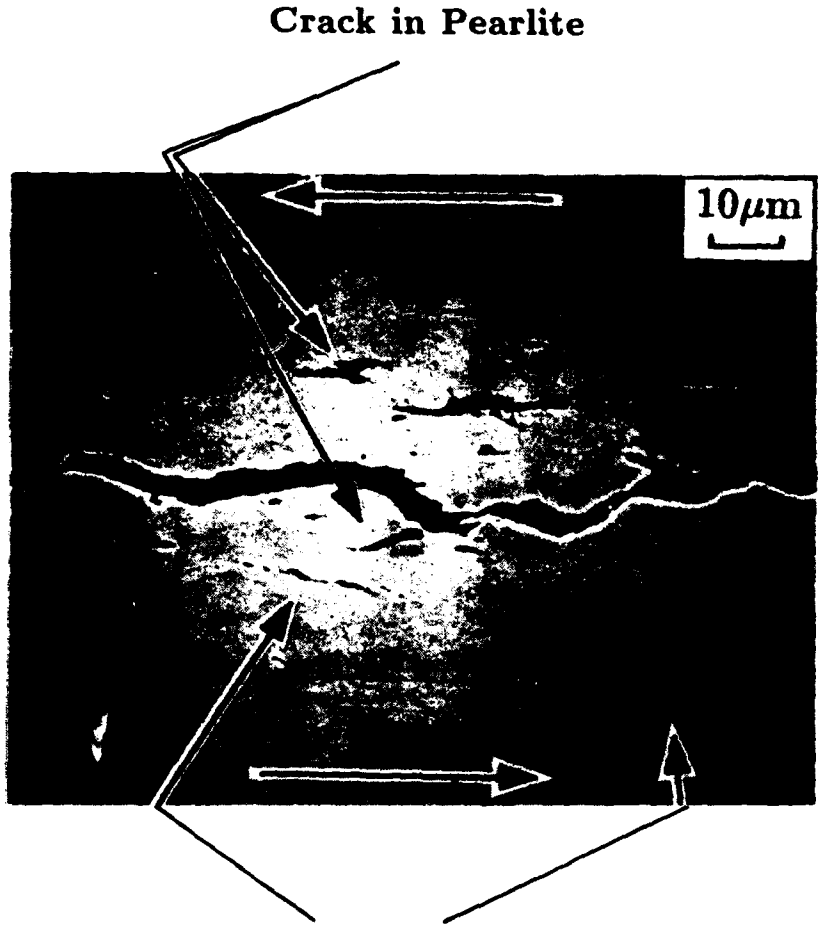

Figure 9. SEM photographs of the shear band in 1018 CRS. The surface is polished but not etched. Figures (a), (b) and (c) correspond to the areas A, B and C, respectively, in Figure 8. The figures show a long arrested crack with smaller microcracks and voids formed within the shear band.

(b)

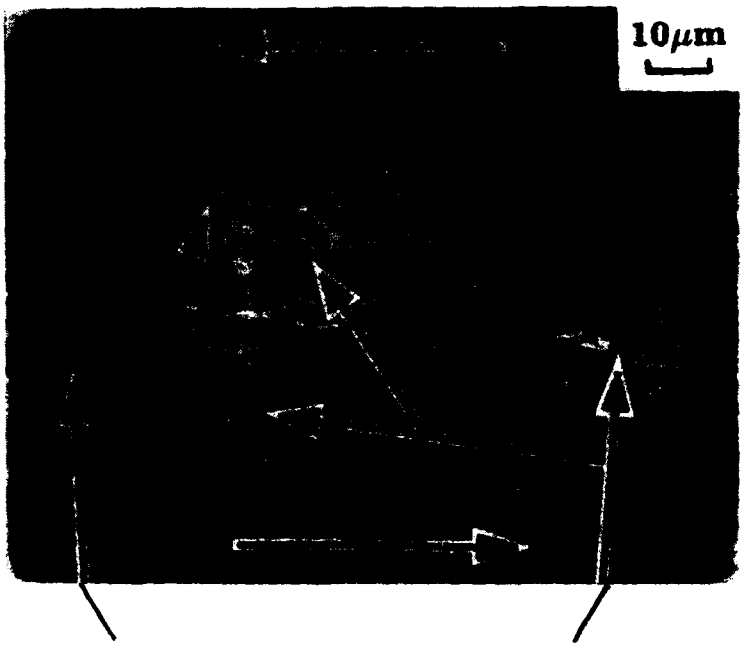

(c) **Crack in Pearlite** **Void at Phase Boundary**

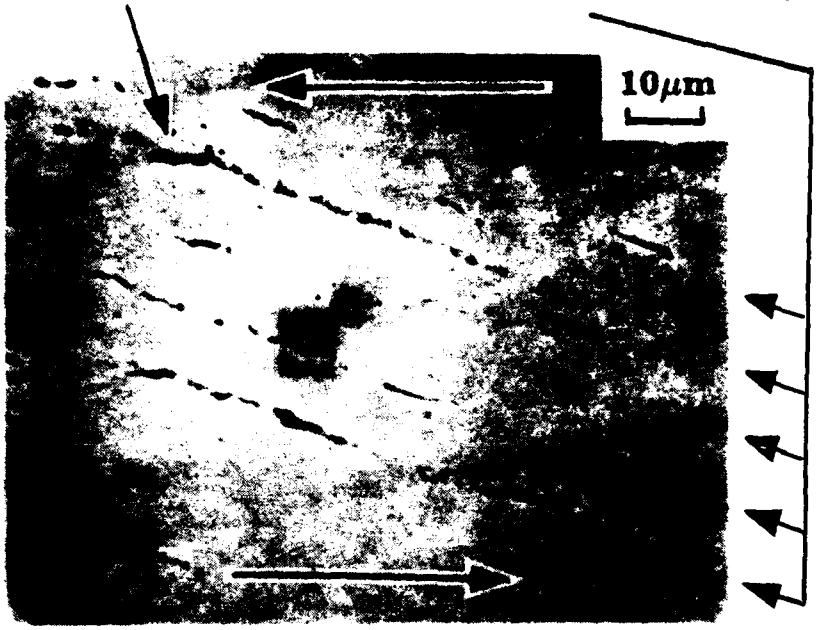

Figure 9 (b) and (c) See Figure 9 for caption.

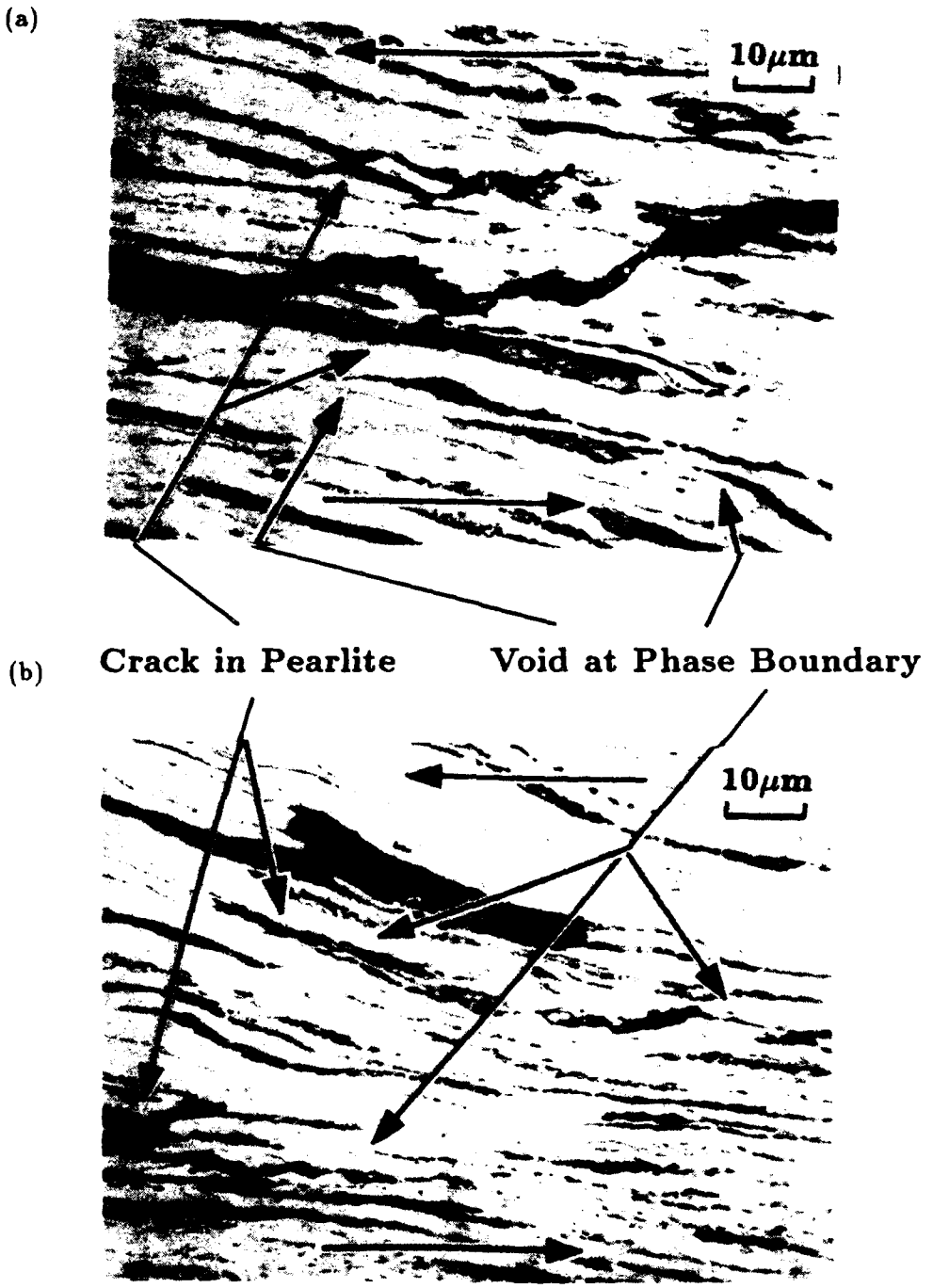

Figure 10. Optical micrographs of the shear band in 1018 CRS. The surface is polished and etched. Figures (a) and (b) correspond to the areas A and B, respectively, in Figure 8. A comparison of corresponding areas in Figures 9 and 10 identifies microcracks and voids. For example, decohesion of the interface between ferrite and pearlite, breaking apart of a pearlite lamella and separation of a ferrite grain boundary.

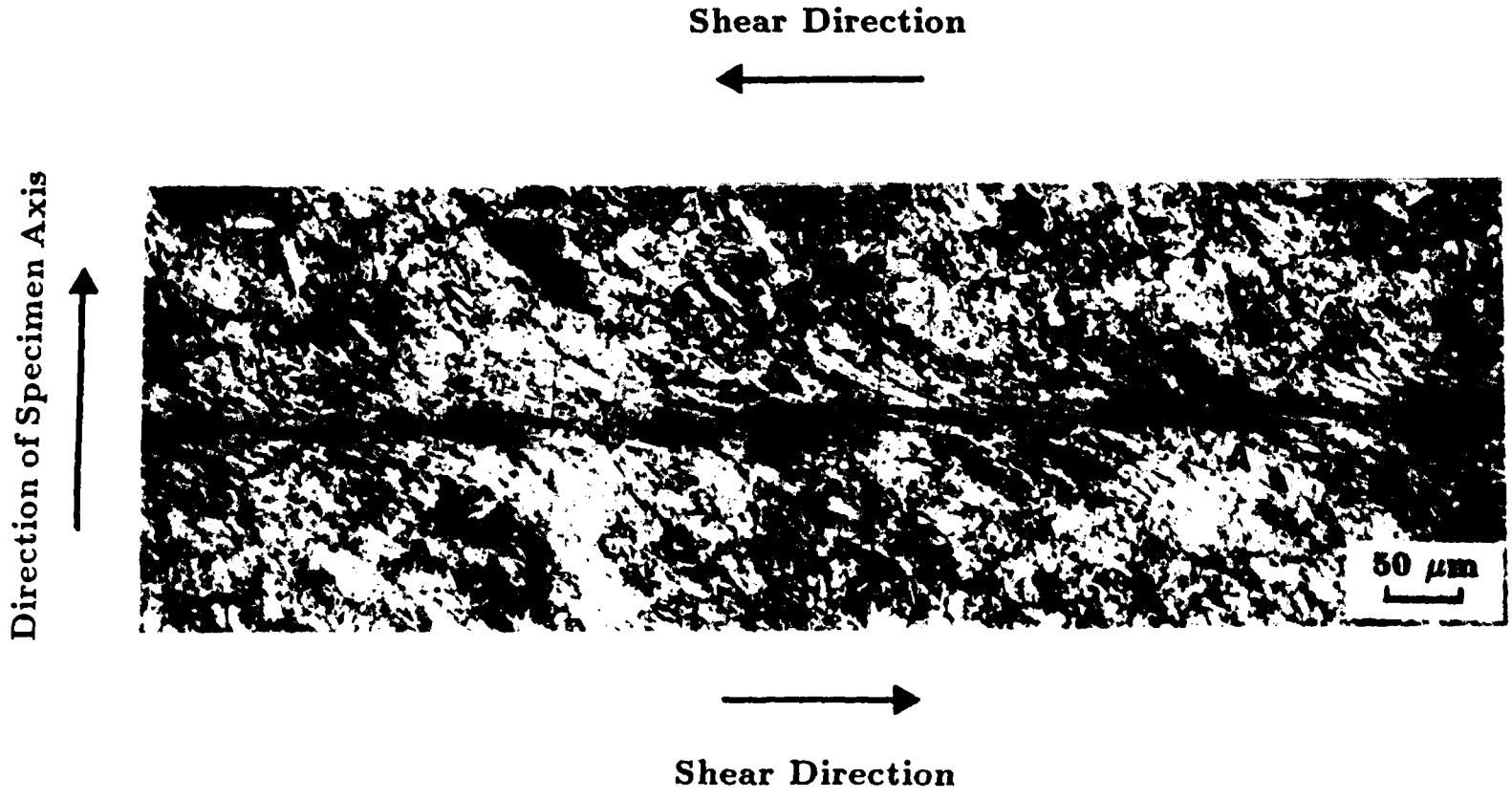

Figure 11. Optical micrographs of a shear band formed in HY-100 steel, after polishing and etching. The higher magnification in (b) of the area A in (a) shows the void linkage within the shear band.

(b)

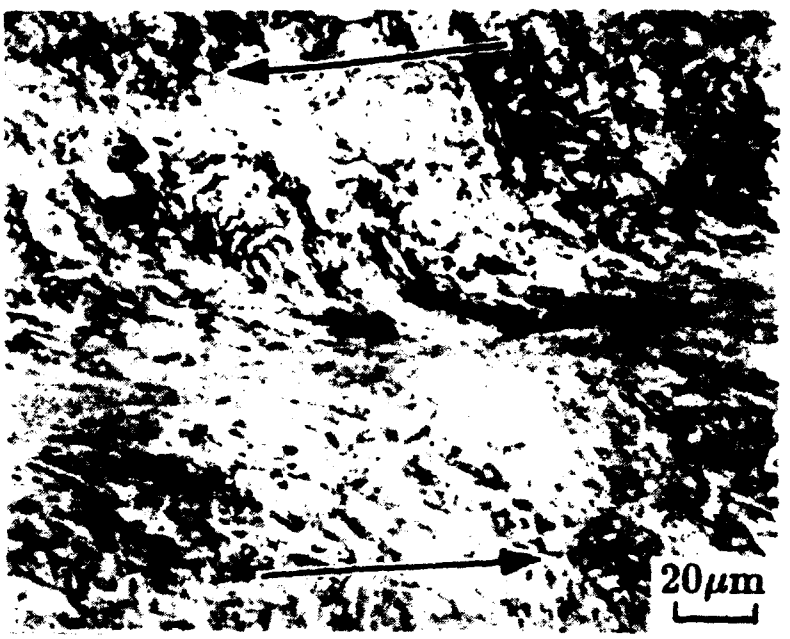

Figure 11 (b) See Figure 11 for caption.

(a)

(b)

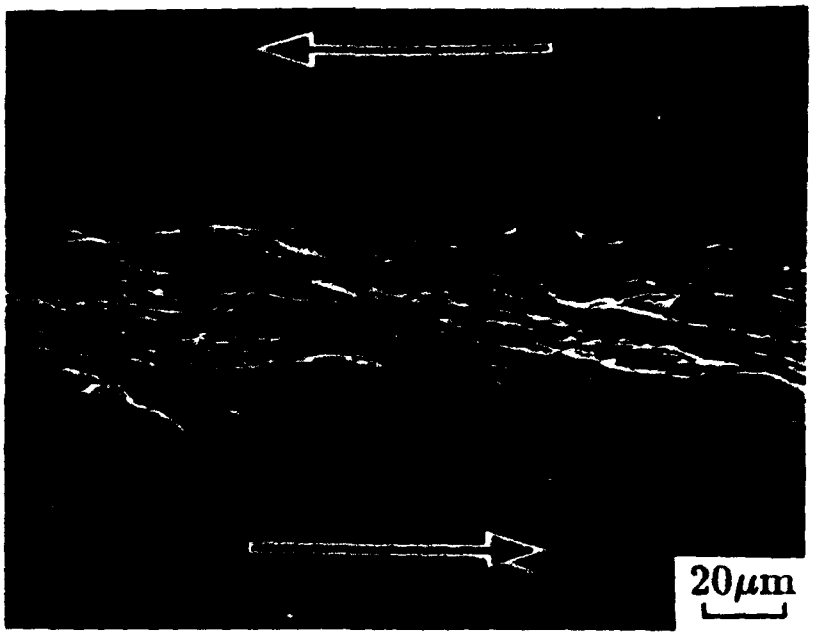

Figure 12. Shear band formed in HY-100 steel. (a) The appearance of the shear band in polarized light microscopy after polishing and etching, showing a white etched region in the center of the shear band and deformed features near its edges. (b) The surface structure of the shear band before polishing and etching, as seen with SEM. Flow lines can be seen within and outside the shear band.

(a)

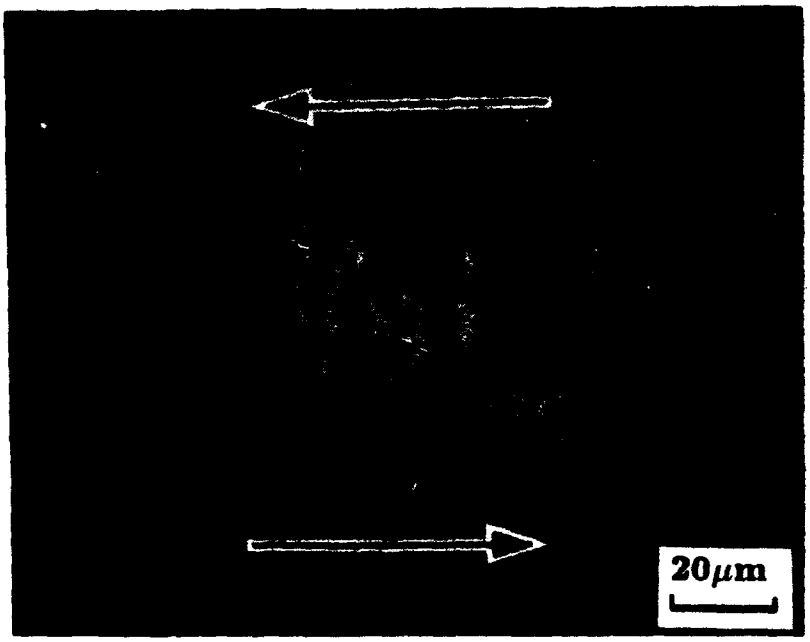

(b)

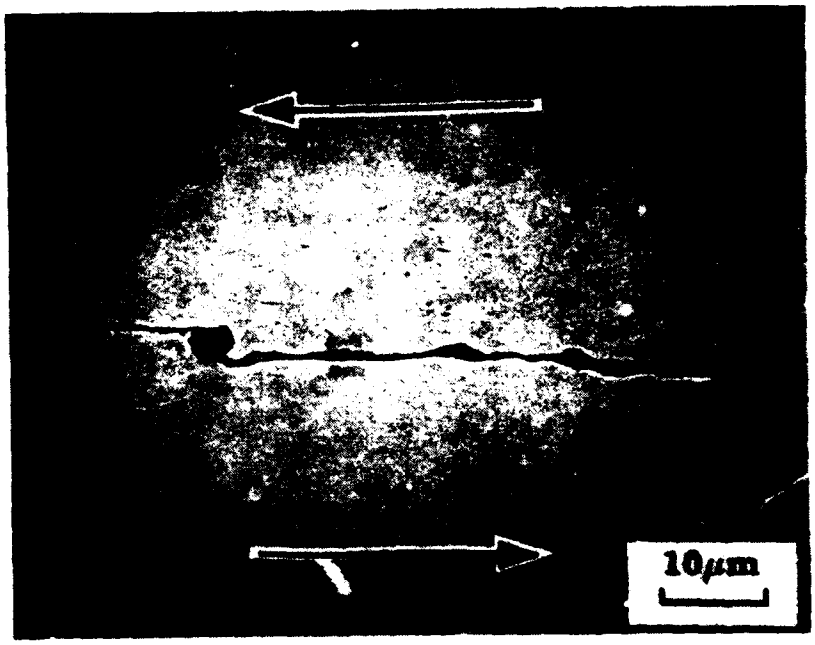

Figure 13. SEM photographs of the polished surface of a shear band in HY-100 steel. (a) Voids formed at MnS inclusions within the shear band, as seen at a low magnification. (b) Linkage of voids formed at globular MnS inclusions. (c) Formation of a void at a MnS stringer; fragments of the stringer appear in the crack. (d) EDAX scan showing the presence of Mn and S within the void in (c).

(c)

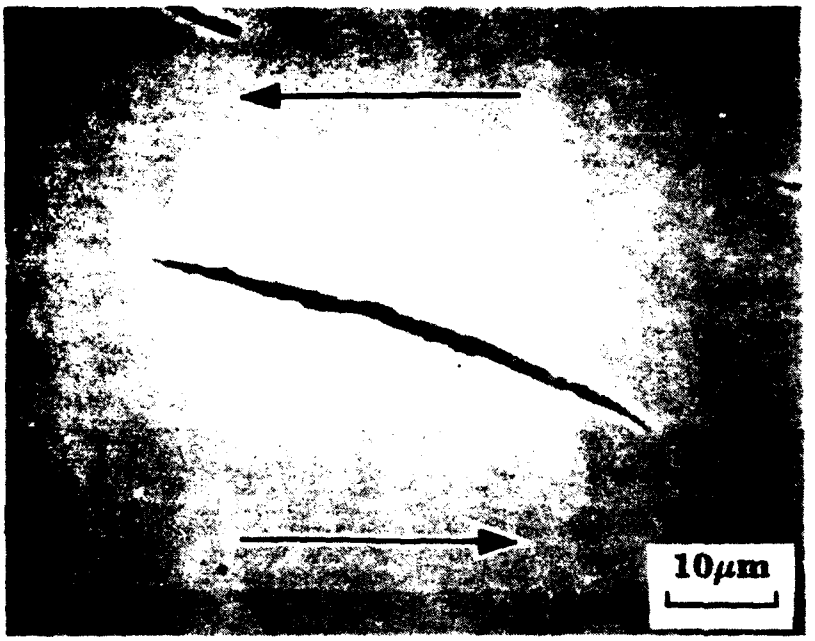

(d)

Figure 13 (c) and (d) See Figure 13 for caption.

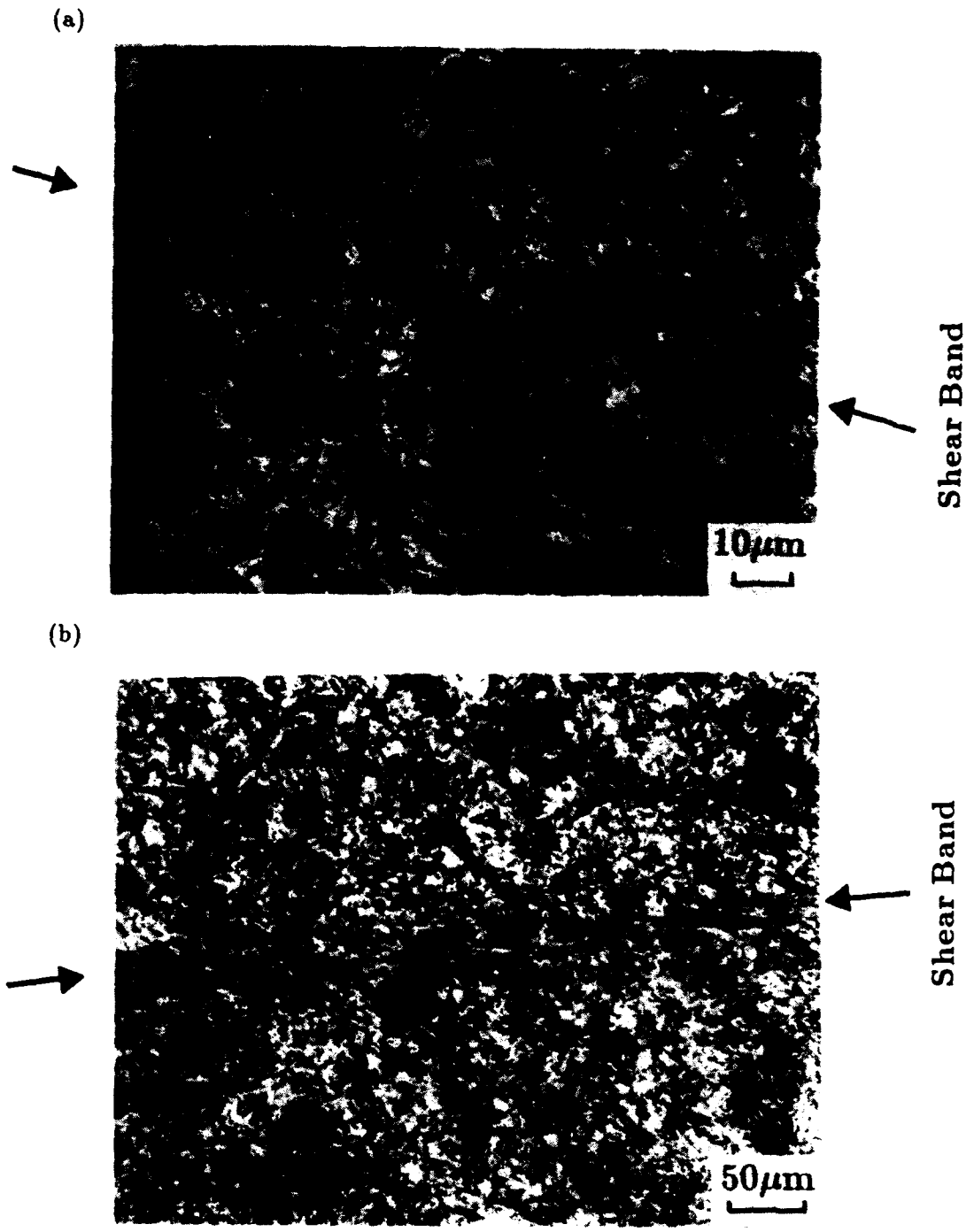

Figure 14. Optical micrographs of transformed shear bands formed in 4340 VAR steel, (a) 200 C temper and (b) 425 C temper. White etched bands whose appearance is accentuated by observation in polarized light are shown in (c) for the 200 C temper and (d) for the 425 C temper.

(c)

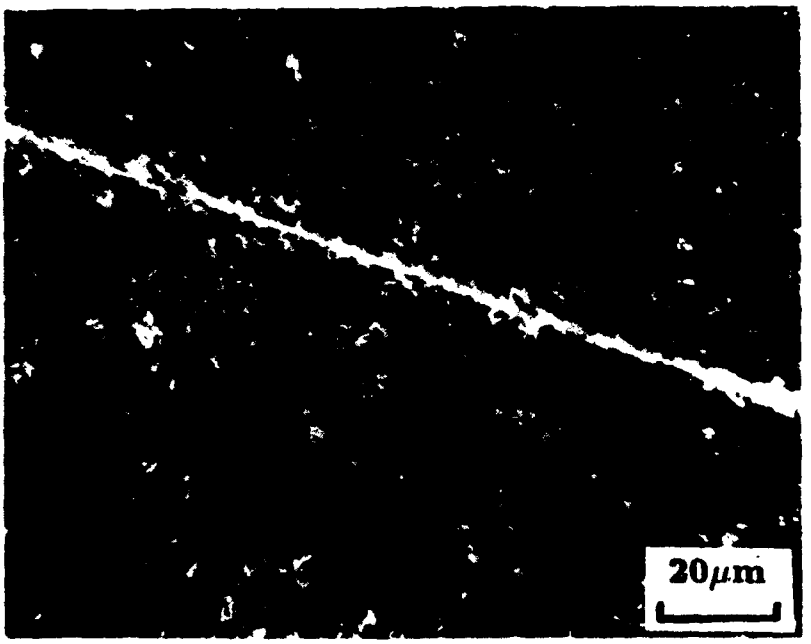

(d)

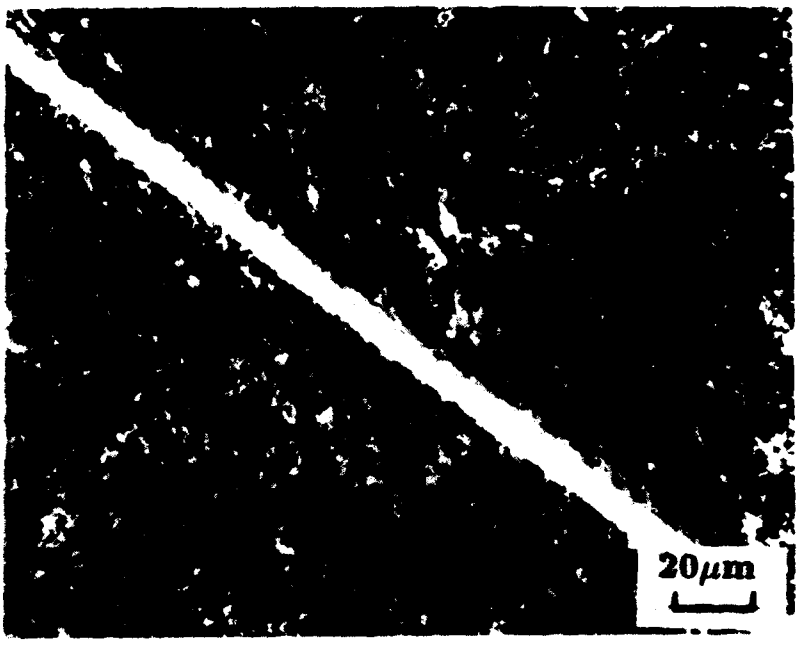

Figure 14 (c) and (d) See Figure 14 for caption

(a)

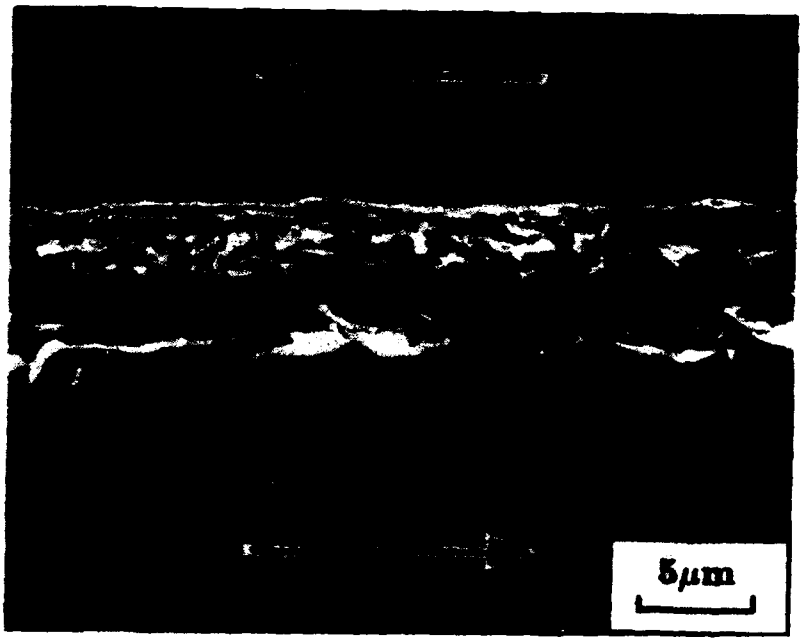

(b)

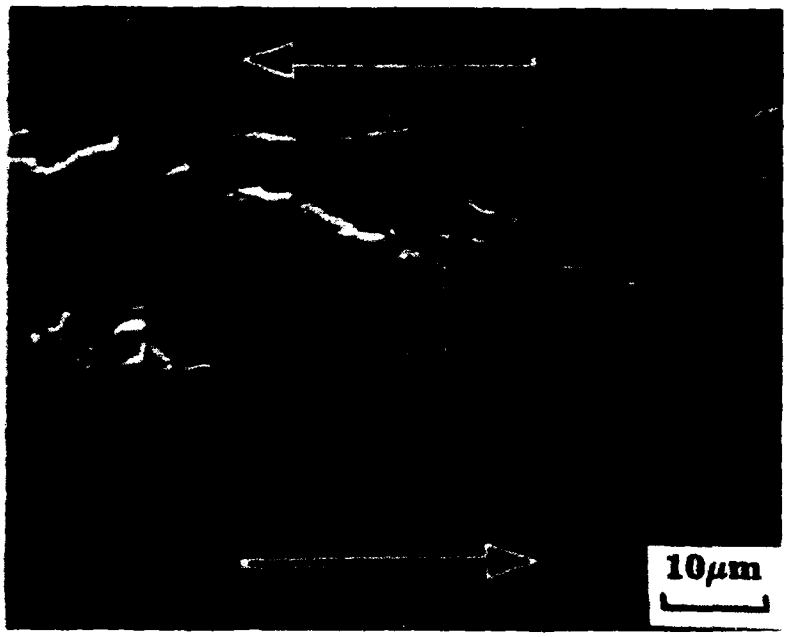

Figure 15. Surface structure of 4340 VAR steel specimens after the formation of a shear band, before polishing and etching, as seen with SEM. (a) the 200 C temper specimen shows sharp edges separating the shear band and the matrix with different features in each. (b) the 425 C temper specimen shows relatively well defined boundaries between the shear band and the matrix.

(a)

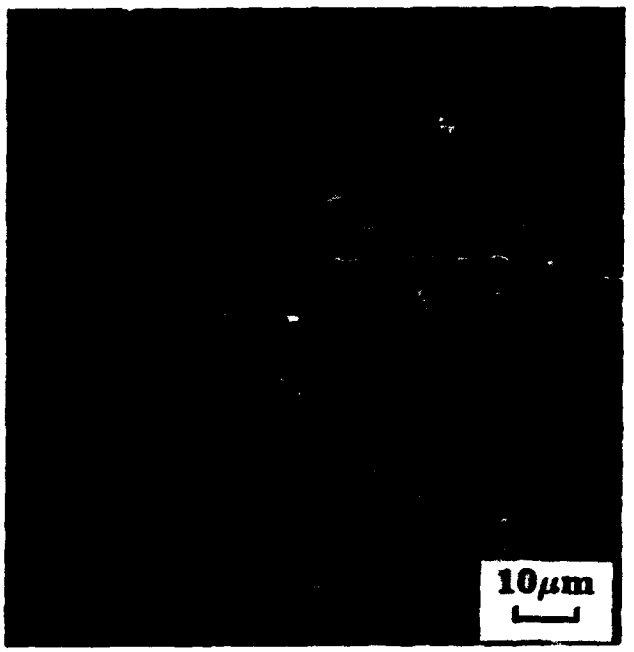

(b)

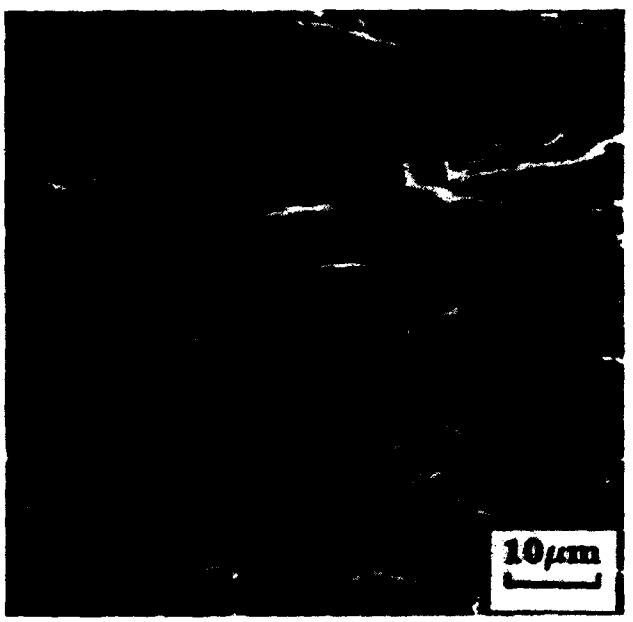

Figure 16. SEM fractographs of 1018 CRS. (a) Elongated ductile dimples typical of parts of the surface area. (b) A smoothed part of the surface area due probably to rubbing against the opposing face of the fracture.

(a)

(b)

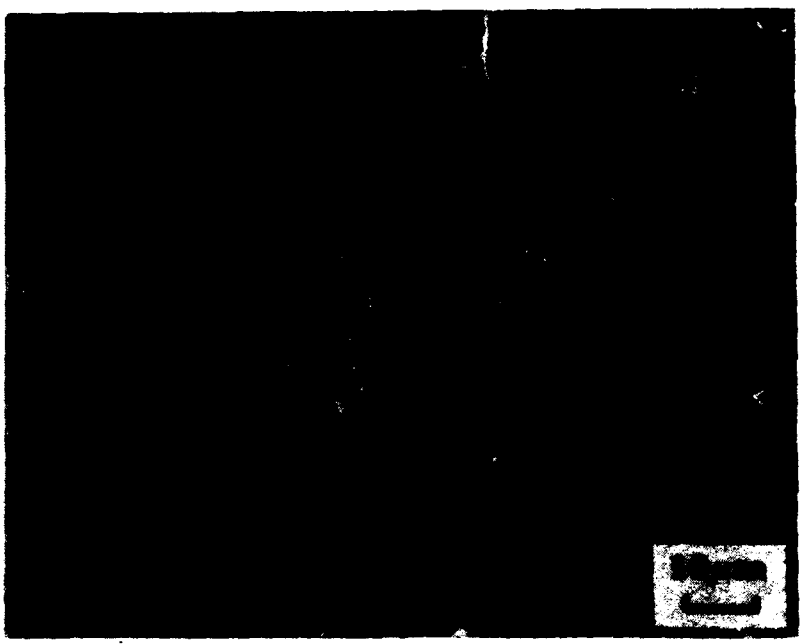

Figure 17. SEM fractographs of HY-100 steel. (a) Elongated ductile dimples showing broken pieces of a MnS stringer within a large elongated dimple. (b) Smoothed surface, some knobbly feature may be seen.

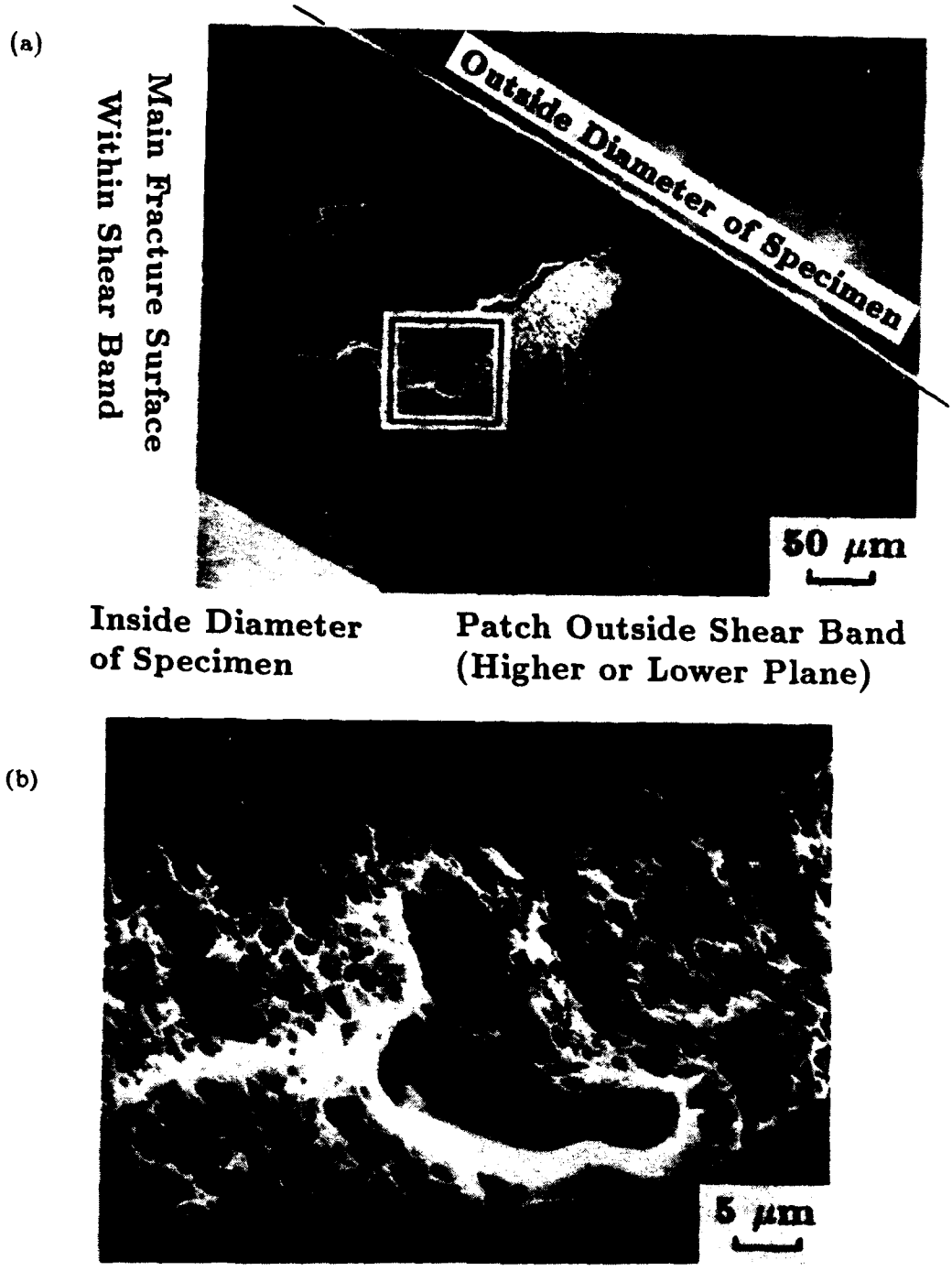

Figure 18. SEM fractographs of 4340 VAR steel, 200 C temper. (a) A patch containing larger dimples, presumably due to the crack path moving outside the plane of the shear band. A magnified view of the square area within the patch is shown in (b). (c) Smaller dimples, which are dominant over the main fracture surface formed within the shear band. (d) smoothed surface area.

(c)

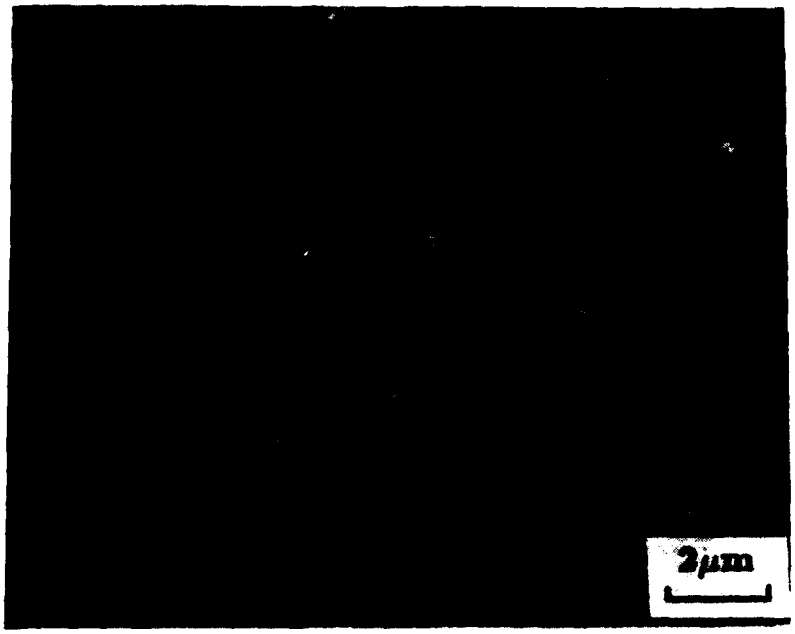

(d)

Figure 18 (c) and (d) See Figure 18 for caption.

(a)

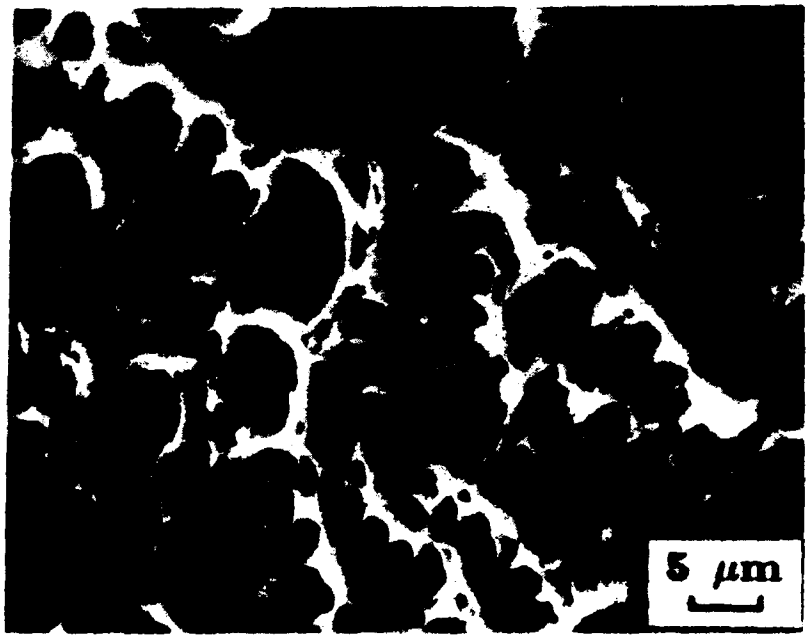

(b)

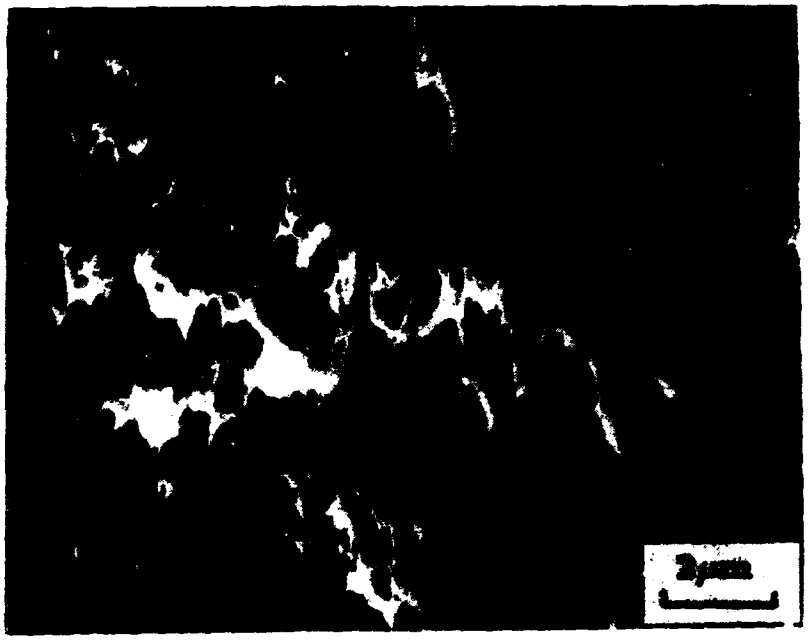

Figure 19. SEM fractographs of 4340 VAR steel, 425 C temper. (a) Larger dimples, (b) smaller elongated dimples typical of most of the fracture surface, (c) knobbly-like features and (d) smoothed surface area.

(a)

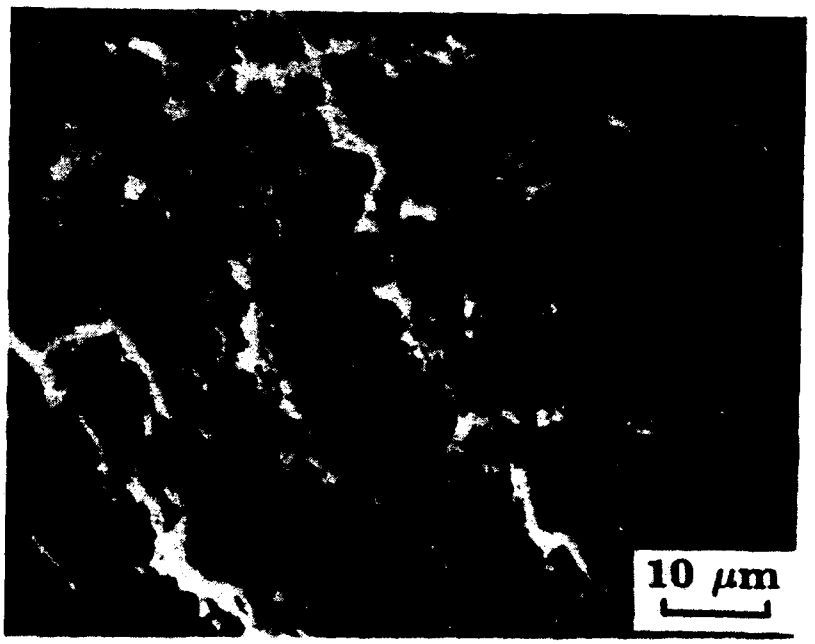

(b)

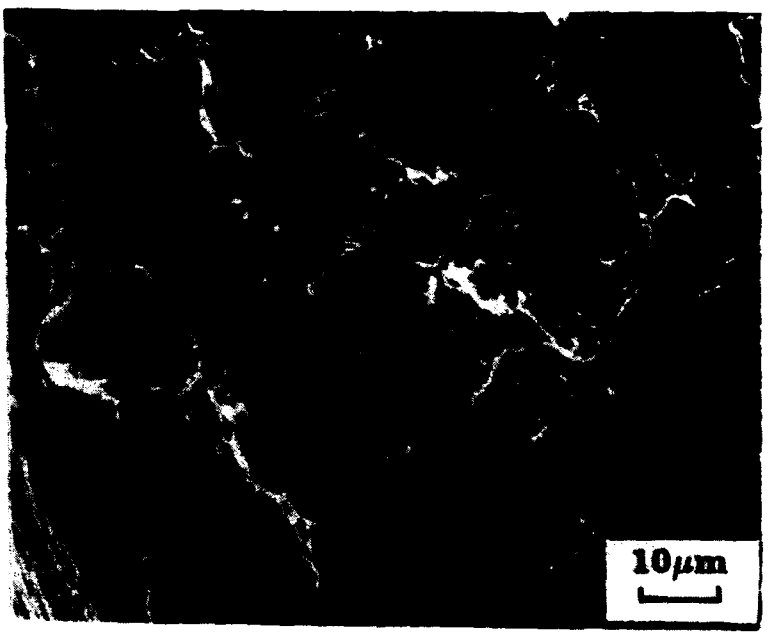

Figure 19 (c) and (d) See Figure 19 for caption.